PONTIFÍCIA UNIVERSIDADE CATÓLICA
DO RIO DE JANEIRO

Raul Ribeiro da Silva

An Optimization-Based Equivalent DC Power Flow Model for Network Reduction

Dissertação de Mestrado

Dissertation presented to the Programa de Pós-Graduação em Engenharia Elétrica of PUC–Rio in partial fulfillment of the requirements for the degree of Mestre em Engenharia Elétrica.

Advisor   :   Prof. Alexandre Street de Aguiar
Co-advisor: Prof. Fernando Adolfo Mancilla David

Rio de Janeiro
May 2020

PONTIFÍCIA UNIVERSIDADE CATÓLICA
DO RIO DE JANEIRO

Raul Ribeiro da Silva

An Optimization-Based Equivalent DC Power Flow Model for Network Reduction

Dissertation presented to the Programa de Pós-Graduação em Engenharia Elétrica of PUC–Rio in partial fulfillment of the requirements for the degree of Mestre em Engenharia Elétrica. Approved by the Examination Committee.

Prof. Alexandre Street de Aguiar
Advisor
Departamento de Engenharia Elétrica – PUC–Rio

Prof. Fernando Adolfo Mancilla David
Co-advisor
University of Colorado Denver – CU Denver

Prof. Alejandro Alberto Angulo Cárdenas
Universidad Técnica Federico Santa María – UTFSM

Prof. Phillipe Vilaça Gomes
Departamento de Engenharia Elétrica – PUC–Rio

Rio de Janeiro, May 12th, 2020

Raul Ribeiro da Silva

Raul Ribeiro da Silva received his B.Sc. degree in Electrical Engineering in 2017 from the Universidade Federal Fluminense (UFF), Brazil. During his undergraduate program, he spent a year as an exchange student at the University of Sydney, Australia. Since 2018, he has been part of the Laboratory of Applied Mathematical Programming and Statistics (LAMPS) in the Department of Electrical Engineering at the Pontifícia Universidade Católica do Rio de Janeiro(PUC-Rio).

Acknowledgments

Abstract

> Ribeiro da Silva, Raul; Street de Aguiar, Alexandre (Advisor); Mancilla–David, Fernando (Co-Advisor). **An Optimization-Based Equivalent DC Power Flow Model for Network Reduction**. Rio de Janeiro, 2020. 66p. Dissertação de Mestrado – Departamento de Engenharia Elétrica, Pontifícia Universidade Católica do Rio de Janeiro.

The use of full model representation in power system studies may lead to undesirable levels of computational burden and inaccuracy due to modern system complexities and uncertainties. To address the tractability issue, network reduction methods aim to create a simplified model, with reduced dimension, of a given power system. Current techniques consider only one operating point in their reduction process, falling short in properly performing for a wide range of operating conditions. Additionally, a nonlinear AC power flow solution features worse computation performance, but better accuracy when compared against its linearized counterpart (DC power flow solution). Unfortunately, the DC power flow approximation disregards the line losses and nonlinear effects due to changes in voltage levels and reactive power.

In this context, we propose a novel optimization–based framework to create equivalent power flow models. Thus, to overcome the computational performance limitations and imprecision for multiple operating scenarios, we use the proposed framework to produce a DC–based network reduction method that performs well in many operating points. The solution of a linear optimization problem, which considers multiple AC power flow scenarios or network measurements, determines the equivalent network parameters. To ensure modeling accuracy, we consider a set of artificial dynamic loads to represent the mismatch between observed scenarios and the response of the equivalent. These artificial loads are polynomial functions of the operating point, and their coefficients are co-optimized with the reduced network parameters. Principal Component Analysis (PCA) is used to extract the relevant components of the load vector defining the operating point, reducing the equivalent model dimensionality, and improving out–of–sample performance. We test the methodology against traditional Ward equivalent for different operating conditions. We present case studies with generated data to investigate the model generalization capability for different noise levels. Finally, we conduct a case study based on realistic load profiles from a Brazilian distribution company within the IEEE 118–Bus test system.

Keywords

Power Systems; Network Reduction; Linear Programming; Power Flow.

Resumo

Ribeiro da Silva, Raul; Street de Aguiar, Alexandre; Mancilla–David, Fernando. **Modelo Equivalente de Fluxo de Potência CC para Redução de Redes Baseado em Otimização**. Rio de Janeiro, 2020. 66p. Dissertação de Mestrado – Departamento de Engenharia Elétrica, Pontifícia Universidade Católica do Rio de Janeiro.

O uso da representação de modelos completos em estudos de sistemas de potência pode levar a indesejados níveis de esforço computacional e imprecisão devido às incertezas e complexidade dos sistemas modernos. Para endereçar este problema de tratabilidade, métodos de redução de redes buscam criar um modelo simplificado, com dimensão reduzida, de um dado sistema de potência. As técnicas atuais consideram apenas um ponto de operação no processo de redução falhando em desempenho para uma grande variedade de condições operativas. Adicionalmente, a solução para o fluxo de potência CA (não linear) apresenta pior performance computacional, mas melhor precisão quando comparada à sua contraparte linear (solução para fluxo de potência CC). Infelizmente, a aproximação do fluxo de potência CC desconsidera a perda de energia nas linhas e os efeitos das não linearidades devido as mudanças nos níveis de tensão e potências reativas no sistema.

Neste contexto, um novo modelo de fluxo de potência equivalente baseado em otimização é proposto. Assim, para superar as limitações relativas a performance computacional e as imprecisões para multiplos cenários operativos, utilizamos o modelo proposto para produzir um método de redução baseado no fluxo CC, que apresenta bom desempenho em variados pontos operativos. Neste caso, a solução de um problema de otimização linear,que considera múltiplos cenários de fluxo CA ou medições do sistema, determina os parâmetros da rede equivalente. Para garantir a precisão do modelo, consideramos um conjunto de cargas artificiais para representar o desbalanço entre os cenários observados e a resposta da rede equivalente. Estas cargas artificiais são funções polinomiais do ponto operativo do sistema, e seus coeficientes são cootimizados com os parâmetros da rede reduzida. A Analise de Componentes Pincipais é utilizada para extrair as componentes relevantes do vetor de cargas que define um ponto operativo, reduzindo a dimensão do modelo, e melhorarando o desempenho *out–of–sample*. A metodologia é testada contra o equivalente Ward para diferentes condições operativas. Casos de estudo com dados gerados são apresentados com o objetivo de analisar a capacidade de generalização do modelo para diferentes níveis de ruído. Por fim, um caso de estudo com perfís de carga realísticos oriundos de uma companhia de distribuição brasileira é conduzido no sistema de teste IEEE 118–Bus.

Palavras-chave

Sistemas de Potência; Redução de Redes; Programação Linear; Fluxo de Potência.

Table of contents

List of figures

List of tables

1
Introduction

Modern power systems are complex and highly interconnected. For planning and operating these systems while minimizing resources and meeting security requirements, a massive number of studies are required, such as transmission planning [1], energy scheduling [2–4], probabilistic load flow studies [5] and others. In these cases, modeling the network through a power flow perspective is mandatory, and for that, the nonlinear AC power flow (AC PF) model is the most trustworthy formulation [6]. Although current technologies offer great processing capabilities, the full representation of these highly dimensioned systems modeled with the nonlinear AC PF formulation still may lead to undesirable levels of computational burden and even non-tractable NP-hard problems. To mitigate these issues, a designer can appeal to some techniques, such as the simplification or relaxation of some network constraints and network reduction, to generate more tractable power systems models.

The use of simplified network models, especially linear formulations, is common in power system analysis. They offer tractable linear models that are scalable and hence can be used in large–scale optimization–based applications [1–4]. Although these linear power flow models feature a smaller computational burden, they present worse accuracy when compared against their AC nonlinear counterpart, as is the case of the DC PF, which does not take into account power losses. Authors in [7, 8] present and compare different linear power flow (PF) approaches. A second alternative in making a network model more tractable is to relax some of its AC PF constraints. This alternative leads to convex sets of constraints but may lead to unrealistic results. Authors in [9,10] describe a great deal of these relaxation methods which are not covered in this work.

Network reduction techniques aim at creating a reduced dimension representation of a given system while keeping acceptable accuracy levels for a given application. The first reports addressing the use of network reduction methods to decrease the computational burden in power system analysis are from the late 1940s. [11]. In subsequent decades, radial equivalent independent (REI) and Ward equivalent methods gained strength with a couple

of improvements as reported in [12–14]. Different reduction approaches were developed to deal with distinct applications, such as on-line security studies [12, 15], stability analysis [16, 17], and economic dispatch. In recent years, network reduction techniques based on optimization have received a great deal of attention [18–22]. Recently, the search for reduction methods capable of properly performing for a wide range of operating points grows in relevance, since this is a deficiency of current approaches.

The majority of the aforementioned reduction techniques rely on external equivalents, which correspond to smaller–dimension structures replacing an entire section of a system that is not the object of study (an external system) but preserving the details of an area of interest. The architecture thus corresponds to an external system, an internal system, and a boundary, made up of the various buses interconnecting these two subsystems. In this context, the area of interest consists of the internal system and the boundary buses.

Thus, the motivation of this research is the proposal of a novel optimization–based framework to derive equivalent PF–based models to facilitate power system analysis in general. These derived models could be linearized or relaxed formulations, reduced network models, or even a combination of them both. The framework itself is a regression–like optimization model that chooses the parameters of the predefined equivalent structure that most fit a set of observed PF data (e.g. PF in some systems branches, voltage angles in specific buses, system total cost) for multiple scenarios. This observed data may come from real measurements or more complete models simulations. The outcome of this approach is an equivalent model that performs similar to the original systems in terms of those observed variables used in the fitting process for multiple scenarios.

In this work, the proposed framework will be exclusively used to generate a DC–based network reduction method that performs well in many operating points. The goal is to combine the previously mentioned benefits from the DC PF formulation and the use of network reduction while mitigating some of their drawbacks, namely power loss disregard and multiple scenario imprecision. For that, the reduced system features new dependent loads in predefined buses that together sum an estimation of the total power loss. Furthermore, as the proposed framework considers multiple scenarios, it naturally addresses the issue regarding reduced network imprecision in different operating conditions.

The reduced equivalent is tested in study cases with generated data to analyze the model generalization capability for different noise levels. Besides, we also conduct cases based on realistic load profiles from a Brazilian distribu-

tion company within the IEEE 118-Bus test system. The results are contrasted against the Ward reduction benchmark.

1.1
Contributions

The main contributions of this work are:

1. The proposal of a novel optimization-based framework with the capability of creating equivalent PF-based models robust to changes in the system operating condition.

2. The proposal of a novel network reduction technique capable of reducing complete AC network models into reduced enhanced-DC network models exclusively for active PF studies. The reduced system preserves an area of interest shared in common with the original network. It disregards all external system lines while distributing all external injection in its boundary buses. Also, new loads are coupled to the system attempting to recover its total power loss, being a combination of polynomial functions of a vector of the system state. A linear optimization problem originated from the last item framework defines the parameters of the resulting network.

1.2
Outline

The reminder of this dissertation is organized as follows. Chapter 2 presents AC PF and DC PF formulations. In sequence, Chapter 3 presents a literature review on network reduction highlighting their different types and applications, along with the description of Ward equivalent, which benchmarks the results of this work. Chapter 4 presents the proposed framework used to derive the Enhanced-DC Network Reduced model fully described in Chapter 5. Finally, results and conclusions are respectively provided in Chapter 6 and Chapter 7. All nomenclature presented is summarized in Appendix A. Appendix B shows the PCA theory.

2
Power Flow Problem

The power flow (PF) formulation is key in power system analysis since it is base for many other problems. For instance, by solving a PF, one can estimate the load flow in all branches of a power network together with its voltage profile. The AC PF approach is derived from Kirchhoff's circuit laws and consists of a set of nonlinear equations relying on information regarding system loads, generation, and topology. However, the nonconvexity inherent to these AC PF equations prevents its wide use in large–scale optimization problems. As an alternative, AC equations can be linearized by some simplifications that result in the so–called DC PF formulation.

The AC PF is usually solved by iterative Newton–based methods and the DC PF by directly solving its set of linear equations. Moreover, it is very convenient and useful to solve these set of equations by modeling them as constraints of an optimization problem. In this manner, any solution for the optimization problem is a solution for the set of equations. Further, we can benefit from this optimization framework by exploring the objective function to drive the PF result, as is the case of the Optimum Power Flow (OPF) where the objective function is related to the total cost of a system dispatch. Additionally, we can couple the optimization–based PF in other models to implement important power system studies as is the case of the SDDP in hydropower dispatch [23, 24].

The following sections presents the AC PF and the DC PF modeled as optimization problems.

2.1
AC Power Flow

The nonlinear AC PF equations can be solved in a optimization model as follows:

$$\underset{\substack{v_k, \theta_k, f_{(k,m)}, p_{(k,m)}, \\ q_{(k,m)}, p_k^G, q_k^G}}{\text{minimize}} \quad \text{any} \tag{2-1a}$$

Subject to:

$$p_{(k,m)} = (A_{(k,m)} v_k)^2 G_{(k,m)} +$$

$$- A_{(k,m)} \, v_k \, v_m \, G_{(k,m)} \cos\left(\theta_k - \theta_m + \Phi_{(k,m)}\right) +$$

$$- A_{(k,m)} \, v_k \, v_m \, B_{(k,m)} \sin\left(\theta_k - \theta_m + \Phi_{(k,m)}\right) \qquad \forall \, (k,m) \in \mathcal{L} \quad \text{(2-1b)}$$

$$q_{(k,m)} = (A_{(k,m)} v_k)^2 (B_{(k,m)} + B^{\text{sh}}_{(k,m)}) +$$

$$- A_{(k,m)} \, v_k \, v_m \, B_{(k,m)} \cos\left(\theta_k - \theta_m + \Phi_{(k,m)}\right) +$$

$$- A_{(k,m)} \, v_k \, v_m \, G_{(k,m)} \sin\left(\theta_k - \theta_m + \Phi_{(k,m)}\right) \qquad \forall \, (k,m) \in \mathcal{L} \quad \text{(2-1c)}$$

$$f_{(k,m)} = p_{(k,m)} + j \, q_{(k,m)} \qquad\qquad\qquad \forall \, (k,m) \in \mathcal{L} \quad \text{(2-1d)}$$

$$- \overline{F}_{(k,m)} \leq f_{(k,m)} \leq \overline{F}_{(k,m)} \qquad\qquad\qquad \forall \, (k,m) \in \mathcal{L} \quad \text{(2-1e)}$$

$$p_k^G = \sum_{m \in \mathcal{B}} p_{(k,m)} + P_k^D \qquad\qquad\qquad \forall \, k \in \mathcal{B} \qquad\quad \text{(2-1f)}$$

$$q_k^G + B_k^{\text{sh}} v_k^2 = \sum_{m \in \mathcal{B}} q_{(k,m)} + Q_k^D \qquad\qquad \forall \, k \in \mathcal{B} \qquad\quad \text{(2-1g)}$$

$$\underline{P}_k \leq p_k^G \leq \overline{P}_k \qquad\qquad\qquad\qquad \forall \, k \in \mathcal{B} \qquad\quad \text{(2-1h)}$$

$$\underline{Q}_k \leq q_k^G \leq \overline{Q}_k \qquad\qquad\qquad\qquad \forall \, k \in \mathcal{B} \qquad\quad \text{(2-1i)}$$

$$\underline{V}_k \leq v_k \leq \overline{V}_k \qquad\qquad\qquad\qquad \forall \, k \in \mathcal{B} \qquad\quad \text{(2-1j)}$$

$$\theta_k = 0 \qquad\qquad\qquad\qquad\qquad \forall \, k \in \mathcal{B}^{\text{ref}} \qquad \text{(2-1k)}$$

where (2-1a) symbolizes that we can have any objective function since we respect AC PF constraints. Equations (2-1b) and (2-1c) respectively define the active and reactive load flow at each branch in $\mathcal{L}$. Both, (k,m) and (m,k) are presented in $\mathcal{L}$ so we can capture the flow coming out from bus k going to bus m, and the flow coming out from bus m going to bus k. These two equations can represent the PF in different circuit elements depending on the transformer tap $(A_{(k,m)})$, phase–shift angle $(\Phi_{(k,m)})$ and π–section shunt susceptance $(b^{\text{sh}}_{(k,m)})$ parameters configuration. These possible elements are:

- π–section power line model defined by $A_{(k,m)} = 1$, $\Phi_{(k,m)} = 0$ and $b^{\text{sh}}_{(k,m)} > 0$.

- Traditional transformer model defined by $A_{(k,m)} \neq 1$, $\Phi_{(k,m)} = 0$ and $b^{\text{sh}}_{(k,m)} = 0$.

- Phase–shifter transformer model defined by $A_{(k,m)} = 1$, $\Phi_{(k,m)} \neq 0$ and $b^{\text{sh}}_{(k,m)} = 0$.

In addition, Equation (2-1d) represents the complex PF in all branches. Constraint (2-1e) establishes power flow limits that are usually related to the branch transmission capacity or other security criteria. Equations (2-1f) and (2-1g) represents the 1st Kirchhoff's law for active and reactive power balance in all system nodes. In (2-1h), the upper and lower limits for the active generation in bus k is defined. For the so called PV (constant active power and voltage) and PQ (constant active and reactive power) buses, we

must have $\underline{P}_k = \overline{P}_k = P_k^G$ forcing p_k^G to be fixed. Similarly, Constraint (2-1i) limits the reactive generation, where for PQ buses, $\underline{Q}_k = \overline{Q}_k = Q_k^G$ to keep q_k^G constant. The same stand for (2-1j) which limits voltage magnitudes. For PV and reference buses, we must fix v_k by imposing $\underline{V}_k = \overline{V}_k$. At last, Equation (2-1k) set reference buses voltage angles to be equal to zero.

The active power loss $p_{(k,m)}^{\text{loss}}$ in a system transmission line (k, m) is inferred from the PF solution. It is the difference between the PF that goes from bus k to bus m and the one that goes from bus m to k.

$$
\begin{aligned}
p_{(k,m)}^{\text{loss}} &= p_{(k,m)} + p_{(m,k)} & (2\text{-}2)\\
&= v_k^2 G_{(k,m)} - v_k v_m [\, G_{(k,m)} \cos(\theta_k - \theta_m) + B_{(k,m)} \sin(\theta_k - \theta_m)] + \\
&\quad + v_m^2 G_{(k,m)} - v_m v_k [\, G_{(k,m)} \cos(\theta_m - \theta_k) + B_{(k,m)} \sin(\theta_m - \theta_k)] & (2\text{-}3)\\
&= G_{(k,m)}(v_k^2 + v_m^2) - v_k v_m G_{(k,m)}\{\cos(\theta_k - \theta_m) + \cos[-(\theta_k - \theta_m)]\} + \\
&\quad\quad - v_k v_m B_{(k,m)}\{\sin(\theta_k - \theta_m) + \sin[-(\theta_k - \theta_m)]\} & (2\text{-}4)\\
&= G_{(k,m)}[v_k^2 + v_m^2 - 2 v_k v_m \cos(\theta_k - \theta_m)] & (2\text{-}5)
\end{aligned}
$$

2.2
DC Power Flow

The DC PF model is a linear approximation of the AC PF equations in (2-1). It completely disregards the reactive PF while the active PF is defined by assuming some simplifications in AC PF equations. The simplifications are:

$$
\sin(\theta_k - \theta_m + \Phi_{(k,m)}) \approx (\theta_k - \theta_m + \Phi_{(k,m)}) \qquad \forall (k, m) \in \mathcal{L} \qquad (2\text{-}6\text{a})
$$

$$
v_k \approx 1 \qquad\qquad\qquad\qquad\qquad\qquad\qquad\quad \forall k \in \mathcal{B} \qquad (2\text{-}6\text{b})
$$

$$
R_{(k,m)} \approx 0 \qquad\qquad\qquad\qquad\qquad\qquad\quad \forall (k, m) \in \mathcal{L} \qquad (2\text{-}6\text{c})
$$

where approximation (2-6a) holds true for very small variations in voltage angles between power lines terminal buses. In addition, we consider that all voltage magnitudes are equal to their base values as shown in (2-6b). Equation (2-6c) is more factual for higher voltage systems were $X_{(k,m)} \ggg R_{(k,m)}$. Further, it implies that

$$
G_{(k,m)} = \frac{R_{(k,m)}}{R_{(k,m)}^2 + jX_{(k,m)}^2} \approx 0 \qquad\qquad \forall (k, m) \in \mathcal{L} \qquad (2\text{-}6\text{d})
$$

$$
B_{(k,m)} = -\frac{X_{(k,m)}}{R_{(k,m)}^2 + jX_{(k,m)}^2} \approx -\frac{1}{X_{(k,m)}} \qquad \forall (k, m) \in \mathcal{L} \qquad (2\text{-}6\text{e})
$$

where Equation (2-6d) applied to (2-5), results in a lossless system ($p_{(k,m)}^{\text{loss}} = 0$).

With all the exposed, we can write the DC PF optimization problem as:

$$\underset{\theta_k, f_{(k,m)}, p_k^G}{\text{minimize}} \quad \text{any} \tag{2-7a}$$

Subject to:

$$f_{(k,m)} = -A_{(k,m)} B_{(k,m)} (\theta_k - \theta_m + \Phi_{(k,m)}) \qquad \forall\, (k,m) \in \mathcal{L} \tag{2-7b}$$

$$-\overline{F}_{(k,m)} \leq f_{(k,m)} \leq \overline{F}_{(k,m)} \qquad \forall\, (k,m) \in \mathcal{L} \tag{2-7c}$$

$$p_k^G = \sum_{m \in \mathcal{B}} f_{(k,m)} + P_k^D \qquad \forall\, k \in \mathcal{B} \tag{2-7d}$$

$$\underline{P}_k \leq p_k^G \leq \overline{P}_k \qquad \forall\, k \in \mathcal{B} \tag{2-7e}$$

$$\theta_k = 0 \qquad \forall\, k \in \mathcal{B}^{\text{ref}} \tag{2-7f}$$

where Equation (2-7b) define the PF in power lines as a function of their susceptance and voltage angle difference. It is directly derived from considering (2-6) in (2-1b). Note that we implicitly considered $f_{(k,m)} = p_{(k,m)}$ since we disregard reactive load flow in the DC PF. Constraints in (2-7c) limit power flows. First Kirchhoff law is represented in (2-7d) while Equation (2-7f) sets the voltage angle equal to zero for all reference buses.

3
Network Reduction

This chapter presents the second fundamental tool used in this work to reduce systems dimensions. First, we present a literature review on network reduction, emphasizing the relevance of the proposed reduction model. In sequence, we formulate the Ward equivalent, which is the technique used to validate our model.

3.1
Literature review

In general, there are two great sets of network reduction techniques, namely dynamic and static network reduction. The dynamic type, as the name indicates, is applied to dynamic studies, which are concern with the transient behavior of a power system in specific situations, such as when the status of some components changes. Similarly, static reduction is used for static analysis, such as online security evaluation, planning, and operation studies. In this work, we only deal with static network reduction, hereinafter referred only as network reduction (NR). Authors in [16, 17, 25, 26] deliver more detailed information regarding dynamic equivalents.

There are two groups of static NR methods, the group of methods with PF purpose and the group of techniques applied for OPF studies. For PF applications, preserving the generation cost characteristics of the whole network is irrelevant since this information is not considered because generation dispatch is a known data. On the other hand, for OPF analysis, the representation of generation costs is mandatory. Because of this, the structure of the reduction process is usually different between this two groups and similar within the groups.

The first type of NR to be developed was the reduced networks for PF purposes. NR methods were mostly applied in AC PF based studies, mainly for online security analysis until the late 1990s [11–17, 25, 27–30]. Their reduction process consists in first, dividing the original system into three regions, namely, the external system, internal system, and the boundary region, which interconnects internal and external system as indicated by Figure 3.1(a). Then, an equivalent structure with a reduced dimension replaces the external

system. In this manner, these reduction methods generally differ from each other by how the external equivalent is designed and how its parameters are defined.

3.1(a): Generic system scheme partitioned in three ares: external system, boundary and internal system.

3.1(b): Reduction scheme where a external equivalent replaces the external system.
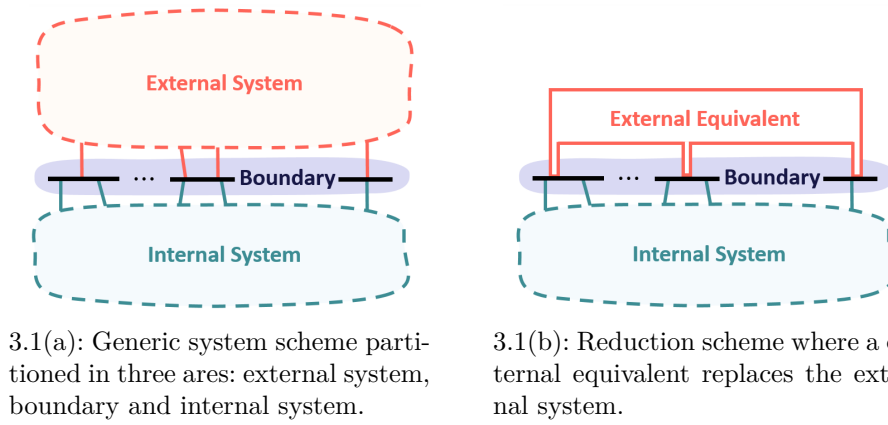
Figure 3.1: Generic power system scheme reduction process.

In the case of Ward reduction, one of the first to be introduced and still largely used in modern practice, the external equivalent is compounded by equivalent lines interconnecting boundary buses, shunts, and injections coupled to the same boundary region [12, 31, 32]. These elements are defined by performing Gaussian elimination in the original system nodal admittance matrix while removing external area elements. Ward model is discussed in detail in Section 3.2. A second famous example of NR for PF analysis is the REI (Radial Equivalent independent) method, which replaces the external system by an equivalent REI node interconnected to the boundary by equivalent lossless power lines. The equivalent node accumulates all external power injection while equivalent lines distribute the total injection to the boundary buses at the same proportion that the external system did. Line susceptances are estimated based on the power incoming and the voltage level at the buses of the boundary [12, 28, 30].

From the 2000s onward, a new form of NR emerged to be compatible with OPF based applications, which require to preserve some generation cost properties. These methods reduction process usually follows two main steps. First, network buses and their loads and generators are aggregated into a smaller set of equivalent buses by a clustering method. It is most common that these clustering methods group together buses that show a similar response for a specific system state (e.g., nodal cost and electrical distance). Then, secondly, equivalent power lines connecting these equivalent buses are created. In general, NR for OPF applications differs from each other by how they

perform the clustering and how is the equivalent lines creation process. Figure 3.2 illustrates the basic structure behind NR for OPF applications.
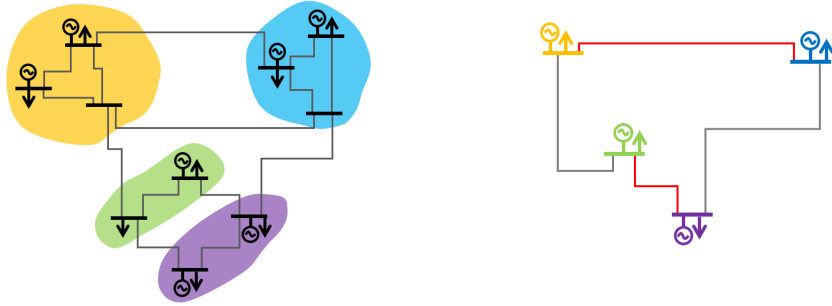
3.2(a): Clustering process where buses are grouped according to some similarity parameter. Here the system is divided in 4 zones

3.2(b): Based in the 4 zones identified in 3.2(a), 4 equivalent nodes are formed. Next, new lines parameters are estimated (in this case the red lines).

Figure 3.2: A 10 bus system reduced into an equivalent 4 bus system for OPF studies.

Table 3.1 puts together a collection of publications regarding NR methods, where each row refers to a piece of work sorted by year of publication in ascending order. A checkmark symbol "✓" indicates that the method described in the referenced paper considers the feature indicated by that column. Notice that columns 3 to 6 refer to some aspects of the reduced method cited, including if it is related to Ward or REI equivalent, if it uses a clustering algorithm to aggregate some system areas or if it is based in Power Transfer Distribution Factors (PTDF). Additionally, columns 7 and 8 refer to the application purpose of the reduction technique, if it is for PF or OPF based studies. Further, columns 9 and 10 indicates if the method reduced network consists of an AC or a DC-based PF formulation. Column 11 points out if a reference proposal utilizes optimization in its reduction process and column 12 if it is built to be robust to changes in the system operating point (OP). At last, some cited publication refers to relevant literature reviews being identified by column 13.

When investigating OPF–based NR publications, we find that literature differs in relation to the clustering method used. Authors in [33] and [26] group buses into zones based in electrical distance metrics, while authors in [34] cluster buses into zones according to their Local Marginal Prices (LMP). In [35] the aggregation occurs by solving the Multicut Problem. Additionally, still in the OPF–based NR field, it is most common to find methods that use the system PTDF matrix to estimate new lines impedance. These methods define their equivalent branches by preserving the PF–injection relation of the

original PTDF for the retained buses. The PTDF originated from the DC approximation results in a linear expression where one can determine the load flow in any system power line by exclusively knowing the power injection in all buses. This linear relation may be misleading. It may give the false notion that the reduced system is robust to changes in the operating point (nodal injections) as is the cases of [22, 36–39]. Such an assumption would only be true if the DC approximation were exact.

To truly build NR models that are accurate in many operating conditions, methods considering multiple scenarios have been proposed. This is the case of developments in [20,33,34] where, after the clustering process, the solution of a regression–like optimization problem considering multiple operating scenarios defines equivalent branches. In this framework, the resulting reduced networks are estimated while minimizing their performance error.

Finally, some interesting methods that result in nonlinear reduced models are proposed. In [40], we have an OPF applied method with the reduction process similar to Ward reduction but the Gaussian elimination is operated in the Jacobian matrix instead. Further, in [41], authors propose three different two–bus equivalent structures based on the Holomorphic Embedding Load Flow Method (HELM), which is a PF formulation that can be directly solved and compares results with the classical Ward reduction for different operating conditions, showing better performance for a more correlated load profile.

Within this context, the two contributions of this work are justified. With the first contribution, which is a general framework to define equivalent model parameters, we intend to motivate its use to determine, with the proper manipulations, the parameters of reduced networks. Its formulation considers many different scenarios in a regression–like parameter estimation framework similar to the contributions in [20, 33, 34] but more general. With the second proposal, we contribute with a new NR method for PF studies. Even though it is not Ward based, the structure of the resulting network derived from it resembles Ward reduced networks. As stated in [32], Ward reduction still plays a fundamental role in power system analysis. Additionally, besides not being designed to deal with the OPF model, Ward's principals are contained in many of modern OPF–based NR, such as in [18, 19, 21, 35]. That being said, the proposed NR has the intention of replacing Ward equivalent in future applications. At last, as a linearized model, it includes an interesting feature of minimizing mismatch concerning AC models, which was not observed in any of the methods present in the literature.

Table 3.1: Network Reduction Literature Review

Paper	Year	Reduction Method				Application		Model		Optimization	Robust to OP	Review
		Ward	REI	Clustering	PTDF	PF	OPF	AC	DC			
[11]	1949	✓	–	–	–	✓	–	✓	–	–	–	–
[12]	1979	✓	–	–	–	✓	–	✓	–	–	–	–
[15]	1979	–	✓	–	–	✓	–	✓	–	–	–	–
[13]	1980	✓	✓	–	–	✓	–	✓	–	–	–	–
[27]	1980	✓	✓	–	–	✓	–	✓	–	–	–	–
[28]	1981	–	✓	–	–	✓	–	✓	–	–	✓	–
[14]	1983	✓	✓	–	–	✓	–	✓	–	–	✓	–
[29]	1987	✓	✓	–	–	✓	–	✓	–	–	–	–
[30]	1989	–	✓	–	–	✓	–	✓	–	–	–	✓
[42]	1995	–	–	–	–	✓	–	✓	–	✓	–	–
[40]	2005	–	–	–	–	–	✓	–	✓	–	–	–
[36]	2010	–	–	✓	✓	–	✓	–	✓	–	–	–
[43]	2010	✓	✓	✓	✓	✓	✓	✓	✓	–	✓	–
[37]	2012	–	–	–	✓	–	✓	✓	–	✓	–	–
[38]	2012	–	–	✓	✓	–	✓	–	✓	–	–	–
[44]	2013	–	–	✓	✓	–	✓	✓	–	–	–	–
[18]	2014	✓	–	–	–	✓	–	✓	✓	✓	✓	–
[45]	2014	✓	✓	✓	✓	–	✓	–	✓	–	✓	✓
[39]	2015	–	–	–	–	✓	–	✓	–	–	–	–
[19]	2015	✓	–	✓	✓	–	✓	✓	✓	✓	✓	–
[33]	2016	–	–	–	–	–	✓	–	✓	✓	✓	–
[41]	2016	–	–	✓	✓	✓	–	✓	–	–	–	–
[34]	2017	–	–	✓	–	–	✓	✓	✓	✓	–	–
[20]	2017	–	–	✓	✓	–	✓	–	✓	✓	✓	–
[21]	2018	✓	–	–	–	–	✓	✓	–	✓	–	–
[35]	2018	✓	–	✓	✓	–	✓	–	✓	✓	✓	–
[22]	2018	–	–	✓	✓	–	✓	✓	✓	✓	✓	–
[32]	2018	✓	–	–	–	✓	–	–	✓	–	–	✓
Proposed	2018	✓	–	–	–	✓	–	✓	✓	✓	✓	–

3.2
Ward equivalent

As presented in the previous section, Ward reduction has a great influence on network reduction literature. This section describes its basic formulation, discusses its possible improvements, and relates it to this work NR proposal.

A linear formulation relating current injections and nodal voltages can be described as follows:

$$\boldsymbol{Y} \cdot \boldsymbol{V} = \boldsymbol{J} \tag{3-1}$$

where $\boldsymbol{Y}$ is the original system nodal admittance matrix, $\boldsymbol{V}$ is a column vector containing the complex voltages across buses and $\boldsymbol{J}$ is a column vector of nodal complex current injections. The elements of $\boldsymbol{Y}$ are described below with the same notation of Section 2.1:

$$Y_{k,m} = -A_{(k,m)} Y_{(k,m)} e^{-j\Phi_{(k,m)}} \tag{3-2a}$$

$$Y_{k,k} = jB_k^{\text{sh}} + \sum_{m \in \mathcal{B}} \left(jB_{(k,m)}^{\text{sh}} + A_{(k,m)}^2 Y_{(k,m)} \right) \tag{3-2b}$$

When a system is partitioned in the three regions described in Figure 3.1(a), Equation (3-1) may be rewritten as:

$$\begin{bmatrix} \boldsymbol{Y}_{\text{EE}} & \boldsymbol{Y}_{\text{EB}} & \boldsymbol{0} \\ \boldsymbol{Y}_{\text{BE}} & \boldsymbol{Y}_{\text{BB}} & \boldsymbol{Y}_{\text{BI}} \\ \boldsymbol{0} & \boldsymbol{Y}_{\text{IB}} & \boldsymbol{Y}_{\text{II}} \end{bmatrix} \cdot \begin{bmatrix} \boldsymbol{V}_{\text{E}} \\ \boldsymbol{V}_{\text{B}} \\ \boldsymbol{V}_{\text{I}} \end{bmatrix} = \begin{bmatrix} \boldsymbol{J}_{\text{E}} \\ \boldsymbol{J}_{\text{B}} \\ \boldsymbol{J}_{\text{I}} \end{bmatrix} \tag{3-3}$$

where subscripts E, B and I refer to submatrices with information regarding external, boundary, and internal systems.

By performing Gaussian elimination on (3-3), external buses can be removed resulting in an equivalent reduced system.

$$\begin{bmatrix} \boldsymbol{Y}_{\text{BB}}^{eq} & \boldsymbol{Y}_{\text{BI}} \\ \boldsymbol{Y}_{\text{IB}} & \boldsymbol{Y}_{\text{II}} \end{bmatrix} \cdot \begin{bmatrix} \boldsymbol{V}_{\text{B}} \\ \boldsymbol{V}_{\text{I}} \end{bmatrix} = \begin{bmatrix} \boldsymbol{J}_{B}^{eq} \\ \boldsymbol{J}_{\text{I}} \end{bmatrix} \tag{3-4a}$$

$$\boldsymbol{Y}_{\text{BB}}^{eq} = \boldsymbol{Y}_{\text{BB}} - \boldsymbol{Y}_{\text{BE}} \boldsymbol{Y}_{\text{EE}}^{-1} \boldsymbol{Y}_{\text{EB}} \tag{3-4b}$$

$$\boldsymbol{J}_{\text{B}}^{eq} = \boldsymbol{J}_{\text{B}} - \boldsymbol{Y}_{\text{BE}} \boldsymbol{Y}_{\text{EE}}^{-1} \boldsymbol{J}_{\text{E}} \tag{3-4c}$$

In the above formulation, $\boldsymbol{Y}_{\text{BB}}^{eq}$ is a submatrix that represents the equivalent components coupled to the boundary and $\boldsymbol{J}_{\text{B}}^{eq}$ the submatrix of equivalent current injections at boundary buses. Current injections in (3-3) are derived from the power injected in the system in a relevant operating point. Consequently, for that point, the load flow at the preserved power lines is equal to the origi-

nal system. However, the same is not true if the system load profile is changed
[31].

The following improvements increase Ward's performance. The inclusion
of buffer zones, which are groups of elements neighboring the boundary that
are preserved in the reduction process to increase performance levels in the
internal area. The retention of relevant external PV buses to improve internal
system voltage accuracy. The maintenance of some external power lines (and
consequently their terminal buses) to guarantee precision in some contingency
scenarios [31,32]. In essence, all of these alternatives do not change the concept
of Ward equivalent, theoretically, we are only adding more elements to the
study area to improve performance in the internal area. As stated at the end
of Section 3.1, this work proposed NR method is meant to be an option to
Ward reduction. That is the reason why in Chapter 6 we only consider Ward
reduction to benchmark our model. We assume that any retention analysis
that could be performed in Ward reduction, could actually be implemented in
our proposed NR.

4
Proposed Framework

In this section, we present our proposed framework to derive equivalent PF-based models with an accurate performance for many scenarios.

The framework objective is to minimize a norm based function of the errors between the assumed observed data and the response of the equivalent model for a user–defined set of PF variables in multiple scenarios, while estimating the parameters of this equivalent model. Therefore, the suggested framework aims at establishing the best approximation of the reference system for a given set of observed data. At this point it is crucial to make clear that this proposed main framework is not an equivalent PF-based model, neither could be a reduced network model, it is exactly an optimization problem that will define the parameters of a proposed equivalent model. Notwithstanding, this work exemplifies this equivalence process by using it to develop reduced network linear PF models.

To present the proposed idea, we use a regression notation. First, we assume that ξ_ω^{obs} represents the vector that stacks all the data (load, generation, and network topology) defining a given scenario of observed operative condition (operating point). For this scenario, we also assume as observed the vector that stacks all the PF variables of interest, $\mathbf{y}_\omega^{obs}$. Therefore, these two vectors are assumed to contain the input and output observation collected from the true system under scenario ω. Then, the equivalent model delivers a prediction for $\mathbf{y}_\omega^{obs}$, namely, $\hat{\mathbf{y}}(\mathbf{x}, \xi_\omega^{obs})$, for a given vector of parameters $\mathbf{x}$. In essence, there is the best set of parameters, namely $\mathbf{x}^*$, that results in the equivalent with the best performance.

Therefore, the proposed optimization–based framework can be seen as a parameter estimation problem for a general regression model. According to the above notation, this estimation problem can be stated as:

$$\min_{\boldsymbol{x} \in \mathcal{X}} \quad \sum_{\omega \in \Omega} \pi_\omega \rho(\boldsymbol{\varepsilon}_\omega) \tag{4-1a}$$

$$\text{s.t:} \quad \boldsymbol{\varepsilon}_\omega = \boldsymbol{y}_\omega^{obs} - \hat{\boldsymbol{y}}(\boldsymbol{x}, \boldsymbol{\xi}_\omega^{obs}) \quad \forall\, \omega \in \Omega \tag{4-1b}$$

where the objective function (4-1a) accounts for the expected value of a norm function of the error components, represented by ρ, associated with all selected

PF variables. Thus, Constraint (4-1b) defines these error components, which are the differences between the observed data $\mathbf{y}_\omega^{obs}$ and the prediction $\hat{\mathbf{y}}(\mathbf{x}, \xi_\omega^{obs})$.

5
Enhanced DC–based Network Reduction

In this section, we present a network reduction method originated from the main framework described by (4-1). It will deliver the parameters of a novel reduced network linear PF model. This linear model is the DC PF problem with the addition of some new dependent loads, which are functions of the original system load profile (represented as the principal components of the vector compounded by all loads). They account for the losses mismatch between the base system (the original system or original model) response, and the response of the reduced DC PF model. Hereinafter, this proposed optimization–based reduction method will be referred to as an enhanced DC–based network reduction (EDC–NR) problem. For the sake of simplicity, we will also refer to the equivalent reduced network model as an enhanced DC PF (EDCPF) model.

The reduction process here described is based in the external area replacement by a smaller dimension equivalent as described in Fig. 3.1. Section 5.1 will present the parameters of the external equivalent and Section 5.2 will formulate the EDCPF model. Then, in Section 5.3, the external equivalent structure and the EDCPF model are couple together to the mainframe of 4-1 formulating a treatable EDC–NR formulation.

5.1
External Equivalent

The external equivalent which integrates the EDCPF model is compounded by the following elements:

5.1.1
New boundary lines

The first feature of the external system to be considered is the new lines connecting boundary buses. The main EDC–NR is responsible to determine the value of these lines susceptances (x_l^B). In the EDCPF, they play the fundamental role of correlating the reduced system boundary buses similarly as the external system does with original system boundary buses. This correlation

is defined by the power flow equation described below:

$$f^N_{(k,m),\omega} = -x^B_{(k,m)}(\theta_{k,\omega} - \theta_{m,\omega}) \qquad \forall\,(k,m) \in \mathcal{L}^N, \omega \in \Omega. \qquad (5\text{-}1)$$

where for all new lines (k, m) at any scenario ω, the voltage angles $(\theta_{k,\omega}$ and $\theta_{m,\omega})$ at the terminal buses, which are boundary buses, are correlated by line (k, m) susceptance $x^B_{(k,m)}$. The set $\mathcal{L}^N$ contains all (k, m) combination of boundary buses. Thus, we are creating all possible power lines connecting these buses, unless $x^B_{(k,m)} = 0$. Figure 5.1 illustrates the proposed equivalent network topology with the new equivalent lines indicated.
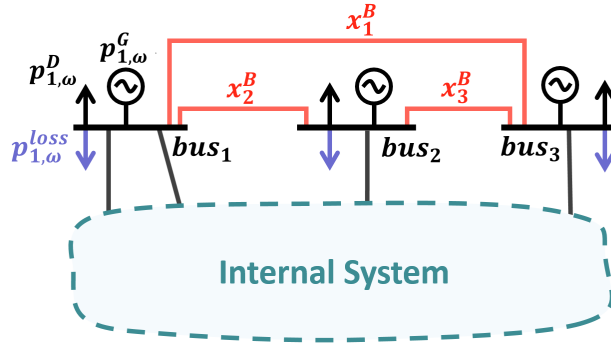
Figure 5.1: Three boundary bus system reduced by an EDC-NR model. The equivalent includes new equivalent lines with susceptances x^B_1, x^B_2 and x^B_3 interconnecting the boundary; three new loads representing mismatch loss; and three new generators and loads due to the allocation of the external injections to the boundary region.

5.1.2
Equivalent loads and generators

In this reduced network, since all external buses are removed, we want to represent these buses active power injection as new equivalent loads and generators coupled to the boundary. In this manner, parcels of each external system load and generator are allocated through the boundary buses by means of parameters $x^G_{i,j}$ and $x^D_{i,j}$. The total allocated load and generation to each boundary bus j in the equivalent model follows the expressions below:

$$0 \leq x^G_{i,j} \leq 1 \qquad \forall\,i \in \mathcal{B}^E, j \in \mathcal{B}^B \qquad (5\text{-}2)$$

$$\sum_{j \in \mathcal{B}^B} x^G_{i,j} = 1 \qquad \forall\,i \in \mathcal{B}^E \qquad (5\text{-}3)$$

$$p^G_{j,\omega} = \sum_{i \in \mathcal{B}^E} P^G_{i,\omega} x^G_{i,j} \qquad \forall\,j \in \mathcal{B}^B, \omega \in \Omega \qquad (5\text{-}4)$$

where Equation (5-2) limits the allocation variables to be between 0 and 1, meaning that we can not allocate more than 100% of an external generation at any boundary bus and that the value of allocation must be positive. In sequence, Expression (5-3) ensures that all external generation will be fully allocated through the boundary and (5-4) defines the equivalent generation at each boundary bus as the summation of all external generation allocated in that bus.

Load allocation follows the same pattern and can be represented by the following set of expressions:

$$0 \leq x_{i,j}^D \leq 1 \qquad \forall\, i \in \mathcal{B}^E,\, j \in \mathcal{B}^B \tag{5-5}$$

$$\sum_{j \in \mathcal{B}^B} x_{i,j}^D = 1 \qquad \forall\, i \in \mathcal{B}^E \tag{5-6}$$

$$p_{j,\omega}^D = \sum_{i \in \mathcal{B}^E} P_{i,\omega}^D\, x_{i,j}^D \qquad \forall\, j \in \mathcal{B}^B,\, \omega \in \Omega \tag{5-7}$$

where Equation (5-5) limits load allocation parameter to be between 0 and 1; Expression (5-6) ensures the full allocation of all external load through the boundary; and (5-7) establishes the new equivalent loads. A short example of the allocation of both, external generation and load, is presented in Figure 5.2. These loads are also represented in the scheme of Figure 5.1.
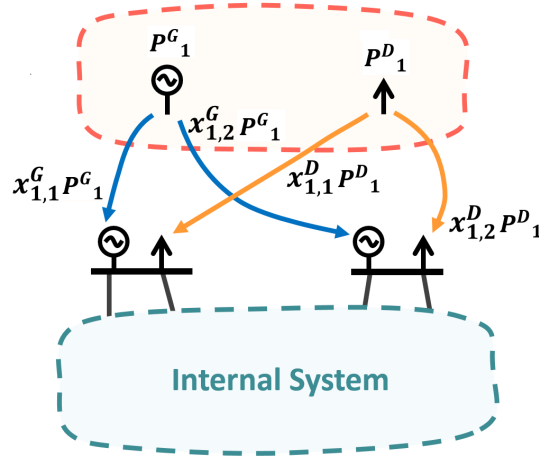

Figure 5.2: Example scheme of external generator and load allocation at the boundary.

5.1.3
Mismatch Loss Function

At last, the proposed EDCPF model features one more new additional active load at each boundary bus. Together, they sum an estimation of the total power loss mismatch that would exist between the base system and the reduced

DC system. The value of each one of these loads is determined by a mismatch function, which is composed of the summation of polynomial functions and it maps the state of the system, returning a parcel of the total power loss mismatch.

In this power flow context, the state of the system can be represented through the vector of all original system loads. However, this vector may present a high dimension for larger systems, therefore, its use as input for the mismatch functions may inflict heavy penalties in computational burden. For this reason, we use a reduced representation of this state vector by recurring to Principal Components Analysis (PCA). Appendix B is fully dedicated to present PCA theory, but we can anticipate that it transforms a set of correlated variables into a smaller set of uncorrelated variables preserving most of the original variation pattern. In this manner, mismatch loss functions are defined as:

$$p_{j,\omega}^{\text{loss}} = \sum_{k=1}^{N_{\text{PC}}} \sum_{n=0}^{N_p} x_{j,n,k}^{\text{loss}} (D_{\omega,k}^{\text{PC}})^n \qquad \forall j \in \mathcal{B}^B, \, \omega \in \Omega \tag{5-8}$$

where N_p is the order of the polynomial functions, N_{PC} is the number of considered components, $D_{\omega,k}^{\text{PC}}$ is the vector of principal components that represents the original system load vector, and all $x_{j,n,k}^{\text{loss}}$ polynomial coefficients are parameters of the reduced network. The example of Figure 5.1 includes mismatch loss loads.

5.2
Enhanced DC Power Flow Model

In this application, as we are only interested in the power flow in some selected lines and in the total power loss recovered through the loss mismatch functions, we define the estimator $\hat{\boldsymbol{y}}^{\text{EDCPF}}(\boldsymbol{x}, \boldsymbol{\xi}_\omega^{obs})$ as the argument of the minimization problem that defines the EDCPF. At this point, we can relate $\boldsymbol{x}$ as the vector that stacks all the parameters of the external equivalent defined in Section 5.1 (all $x_{(k,m)}^B$, $x_{i,j}^G$, $x_{i,j}^D$ and $x_{j,n,k}^{\text{loss}}$). In addition, the vector $\boldsymbol{\xi}_\omega^{obs}$, which defines a scenario ω, is the vector that stacks all base system loads and generation observed ($P_{k,\omega}^G, P_{k,\omega}^D \, \forall k \in \mathcal{B}$).

$$\hat{\boldsymbol{y}}^{\text{EDCPF}}(\boldsymbol{x}, \boldsymbol{\xi}_\omega^{obs}) = (f_{(k,m),\omega}, p_\omega^{\text{loss}})^* \in \underset{\substack{p_{j,\omega}^G, p_{j,\omega}^D, p_{j,\omega}^{\text{loss}}, \theta_{b,\omega}, \\ f_{(k,m),\omega}, f_{(k,m),\omega}^N}}{\arg\min} \quad 1 \tag{5-9a}$$

Subject to:

$$p_{j,\omega}^G = \sum_{i \in \mathcal{B}^E} P_{i,\omega}^G \, x_{i,j}^G \qquad\qquad \forall j \in \mathcal{B}^B \quad \text{(5-9b)}$$

$$p_{j,\omega}^d = \sum_{i \in \mathcal{B}^E} P_{i,\omega}^D \, x_{i,j}^D \qquad\qquad \forall\, j \in \mathcal{B}^B \quad \text{(5-9c)}$$

$$p_{j,\omega}^{\text{loss}} = \sum_{k=1}^{N_{\text{PC}}} \sum_{n=0}^{N_p} x_{j,n,k}^{\text{loss}} (D_{\omega,k}^{\text{PC}})^n \qquad \forall\, j \in \mathcal{B}^B \quad \text{(5-9d)}$$

$$f_{(k,m),\omega}^N = -x_{(k,m)}^B (\theta_{k,\omega} - \theta_{m,\omega}) \qquad \forall\, l \in \mathcal{L}^N \quad \text{(5-9e)}$$

$$P_{j,\omega}^G + p_{j,\omega}^G = P_{j,\omega}^D + p_{j,\omega}^D +$$
$$+ p_{j,\omega}^{\text{loss}} + \sum_{m \in \mathcal{B}} \left(f_{(j,m),\omega} + f_{(j,m),\omega}^N \right) \qquad \forall\, j \in \mathcal{B}^B \quad \text{(5-9f)}$$

$$f_{(k,m),\omega} = -B_{(k,m)} (\theta_{k,\omega} - \theta_{m,\omega} + \Phi_{(k,m),\omega}) \quad \forall\, (k,m) \in \mathcal{L} \tag{5-9g}$$

$$-\overline{F}_{(k,m)} \le f_{(k,m),\omega} \le \overline{F}_{(k,m)} \qquad \forall\, (k,m) \in \mathcal{L}^I \tag{5-9h}$$

$$P_{k,\omega}^G = P_{k,\omega}^D + \sum_{m \in \mathcal{B}} f_{(k,m),\omega} \qquad \forall\, k \in \mathcal{B}^I \quad \text{(5-9i)}$$

$$p_{k,\omega}^G = P_{k,\omega}^D + \sum_{m \in \mathcal{B}} f_{(k,m),\omega} \qquad \forall\, k \in \mathcal{B}^{\text{ref}} \quad \text{(5-9j)}$$

$$\theta_{k,\omega} = 0 \,,\; g_{k,\omega}^{\text{ref}} \ge 0 \qquad \forall\, k \in \mathcal{B}^{\text{ref}} \tag{5-9k}$$

where the objective function in (5-9a) is set to 1 as in the PF problem we want to gouge results by fulfilling constraints rather than achieving a specific objective. Additionally, (5-9b) and (5-9c) define the equivalent loads and generators originated from the allocation of external injection to the boundary. Equation 5-9d define the mismatch loss loads and Equation 5-9e formulate the active load flow at the equivalent lines. Constraint 5-9f is the 1st Kirchhoff Law for boundary nodes. Constraints 5-9g, 5-9h, and 5-9i respectively define power flow in internal system branches, the limits for these same branches, and 1st Kirchhoff Law for nodes in the internal system. At last, reference buses receive especial treatment since its generation is a decision variable as established in 5-9k. Additionally, 1st Kirchhoff Law for them is defined in 5-9j.

5.3
Enhanced DC Network Reduction Model

In this section, we present the mathematical formulation for the proposed EDC–NR optimization model. As exposed in section 5.2, the resulting EDCPF model's purpose is to return similar load flows for some selected power lines only, while preserving the base system total power loss. Thus, $\boldsymbol{y}_\omega^{\text{obs}}$ is the vector that stacks all selected lines PF ($F_{(k,m),\omega}^s$) and the total power loss (P_ω^{loss}) for a given scenario ω. Likewise, the reduced EDCPF (the estimator $\hat{\boldsymbol{y}}$) must return a vector that stacks the estimation of these same values, selected lines

PF ($f^s_{(k,m),\omega}$) and the total power loss (p^{loss}_ω).Thus, we chose to formulate an objective function that is the expected value of the linear combination between the ℓ_1–norm of the error vector associated with the selected lines PF and the absolute value of the total power loss error. With all the exposed, (4-1) is reformulated as:

$$\min_{\boldsymbol{x}\in\mathcal{X}} \quad \sum_{\omega\in\Omega} \pi_\omega \left[\lambda \, ||\boldsymbol{\varepsilon}^F_\omega||_1 + (1-\lambda)|\varepsilon^{\text{loss}}_\omega| \right] \tag{5-10a}$$

$$\text{s.t:} \quad \begin{bmatrix} \boldsymbol{\varepsilon}^F_\omega \\ \varepsilon^{\text{loss}}_\omega \end{bmatrix} = \begin{bmatrix} \boldsymbol{F}^s_\omega \\ D^{loss}_\omega \end{bmatrix} - \hat{\boldsymbol{y}}^{\text{EDCPF}}(\boldsymbol{x}, \boldsymbol{\xi}^{obs}_\omega) \quad \forall\,\omega\in\Omega \tag{5-10b}$$

The bilevel problem described in (5-10) can be further modeled as a single linear optimization problem through the use of some strategies. First, we linearize the absolute value based terms ($||\boldsymbol{\varepsilon}^F_\omega||_1 = \sum_{(k,m)\in\mathcal{L}^s} |\varepsilon^F_{(k,m),\omega}|$ and $|\varepsilon^{\text{loss}}_\omega|$) in the objective function 5-10a by considering auxiliary constrained variables $\delta^F_{(k,m),\omega}$ and $\delta^{\text{loss}}_\omega$ that will assume these values. The estimator in (5-10b) is the EDCPF response presented in (5-9). Note that it is the argument of a minimization problem with a unitary objective function. In this manner, by respecting its constraints, we can couple estimation $\hat{\boldsymbol{y}}^{\text{EDCPF}}(\boldsymbol{x}, \boldsymbol{\xi}^{obs}_\omega)$, for any ω, in an optimization problem. In summary, the EDC-NR problem can be formulated as follows:

$$\min_{\substack{x^B_{(k,m)},x^G_{i,j},x^D_{i,j},x^{\text{loss}}_{j,n,k}, \\ \theta_{k,\omega},p^G_{k,\omega},p^D_{j,\omega},f^N_{(k,m),\omega}, \\ f_{(k,m),\omega},\delta^F_{(k,m),\omega},p^{\text{loss}}_j,\delta^{\text{loss}}_\omega}} \quad \sum_{\omega\in\Omega} \frac{1}{|\Omega|} \left[\lambda \sum_{(k,m)\in\mathcal{L}^s} \delta^F_{(k,m),\omega} + (1-\lambda)\delta^{\text{loss}}_\omega \right] \tag{5-11a}$$

Subject to:

$$\delta^F_{(k,m),\omega} \geq \frac{f_{(k,m),\omega} - F_{(k,m),\omega}}{|\mathcal{L}^S|\overline{F}_{(k,m)}} \qquad \forall\,(k,m)\in\mathcal{L}^S,\,\omega\in\Omega \tag{5-11b}$$

$$\delta^F_{(k,m),\omega} \geq \frac{F_{(k,m),\omega} - f_{(k,m),\omega}}{|\mathcal{L}^S|\overline{F}_{(k,m)}} \qquad \forall\,(k,m)\in\mathcal{L}^S,\,\omega\in\Omega \tag{5-11c}$$

$$\delta^{\text{loss}}_\omega \geq \frac{P^{\text{loss}}_\omega - \sum_{j\in\mathcal{B}^B} p^{\text{loss}}_{j,\omega}}{P^{\text{loss}}_{\max}} \qquad \forall\,\omega\in\Omega \tag{5-11d}$$

$$\delta^{\text{loss}}_\omega \geq \frac{\sum_{j\in\mathcal{B}^B} p^{\text{loss}}_{j,\omega} - P^{\text{loss}}_\omega}{P^{\text{loss}}_{\max}} \qquad \forall\,\omega\in\Omega \tag{5-11e}$$

$$0 \leq x^G_{i,j} \leq 1 \qquad \forall\,i\in\mathcal{B}^E,\,j\in\mathcal{B}^B \tag{5-11f}$$

$$0 \leq x^D_{i,j} \leq 1 \qquad \forall\,i\in\mathcal{B}^E,\,j\in\mathcal{B}^B \tag{5-11g}$$

$$\sum_{i\in\mathcal{B}^E} x^G_{i,j} = 1 \qquad \forall\,j\in\mathcal{B}^B \tag{5-11h}$$

$$\sum_{i \in \mathcal{B}^E} x_{i,j}^D = 1 \qquad\qquad \forall j \in \mathcal{B}^B \qquad\qquad (5\text{-}11\text{i})$$

$$p_{j,\omega}^G = \sum_{i \in \mathcal{B}^E} P_{i,\omega}^G x_{i,j}^G \qquad\qquad \forall j \in \mathcal{B}^B,\, \omega \in \Omega \qquad\qquad (5\text{-}11\text{j})$$

$$p_{j,\omega}^D = \sum_{i \in \mathcal{B}^E} P_{i,\omega}^D x_{i,j}^D \qquad\qquad \forall j \in \mathcal{B}^B,\, \omega \in \Omega \qquad\qquad (5\text{-}11\text{k})$$

$$p_{j,\omega}^{\text{loss}} = \sum_{k=1}^{N_{\text{PC}}} \sum_{n=0}^{N_p} x_{j,n,k}^{\text{loss}} (D_{\omega,k}^{\text{PC}})^n \qquad\qquad \forall j \in \mathcal{B}^B,\, \omega \in \Omega \qquad\qquad (5\text{-}11\text{l})$$

$$f_{(k,m),\omega}^N = -x_{(k,m)}^B (\Theta_{k,\omega} - \Theta_{m,\omega}) \qquad\qquad \forall (k,m) \in \mathcal{L}^N,\, \omega \in \Omega \qquad (5\text{-}11\text{m})$$

$$(1 - \alpha_\theta)\Theta_{j,\omega} \leq \theta_{j,\omega} \leq (1 + \alpha_\theta)\Theta_{j,\omega} \qquad\qquad \forall j \in \mathcal{B}^B,\, \omega \in \Omega \qquad\qquad (5\text{-}11\text{n})$$

$$P_{j,\omega}^G + p_{j,\omega}^G = P_{j,\omega}^D + p_{j,\omega}^D +$$
$$+ p_{j,\omega}^{\text{loss}} + \sum_{m \in \mathcal{B}} \left(f_{(j,m),\omega} + f_{(j,m),\omega}^N \right) \qquad \forall j \in \mathcal{B}^B,\, \omega \in \Omega \qquad\qquad (5\text{-}11\text{o})$$

$$f_{(k,m),\omega} = -B_{(k,m)} (\theta_{k,\omega} - \theta_{m,\omega} + \Phi_{(k,m),\omega}) \qquad \forall (k,m) \in \mathcal{L}^I \cup \mathcal{L}^B,\, \omega \in \Omega$$
$$(5\text{-}11\text{p})$$

$$-\overline{F}_{(k,m)} \leq f_{(k,m),\omega} \leq \overline{F}_{(k,m)} \qquad\qquad \forall (k,m) \in \mathcal{L}^I,\, \omega \in \Omega \qquad (5\text{-}11\text{q})$$

$$P_{k,\omega}^G = P_{k,\omega}^D + \sum_{m \in \mathcal{B}} f_{(k,m),\omega} \qquad\qquad \forall k \in \mathcal{B}^I,\, \omega \in \Omega \qquad\qquad (5\text{-}11\text{r})$$

$$p_{k,\omega}^G = p_{k,\omega}^D + \sum_{m \in \mathcal{B}} f_{(k,m),\omega} \qquad\qquad \forall k \in \mathcal{B}^{\text{ref}},\, \omega \in \Omega \qquad\qquad (5\text{-}11\text{s})$$

$$\theta_{k,\omega} = 0,\, p_{k,\omega}^G \geq 0 \qquad\qquad \forall k \in \mathcal{B}^{\text{ref}},\, \omega \in \Omega \qquad\qquad (5\text{-}11\text{t})$$

where the first term inside brackets in (5-11a) accounts for the ℓ_1–norm of the vector that stacks all selected lines normalized PF error in scenario ω. The second term refers to the absolute value of the total loss estimation error. Note that $0 \leq \lambda \leq 1$ acts as a regularization penalty factor. By decreasing its value, the estimation problem gives up perfectly fitting the selected PF variables to the in–sample observations to obtain a better representation of the total system losses, which may result in better out–of–sample performance. Further, (5-11b)–(5-11e) are used to produce the normalized absolute values metrics for both deviations, the PF (among all scenarios and selected lines), and the system power losses. Constraints (5-11f)–(5-11i) involve the decision variables related to external equivalent parameters, accounting for the term $\boldsymbol{x} \in \mathcal{X}$ in Expression (5-10a). Constraints (5-11j)–(5-11t) are the coupling of all EDCPF constraints (5-9b)–(5-9k) for all scenarios ω. Because (5-9e) relies on bilinear expressions when $x_{(k,m)}^B$ is a decision variable, we make a linear approximation in the model only for the boundary buses. In that case, we replace the angle variables $\theta_{\cdot,\omega}$ by their observed values $\Theta_{\cdot,\omega}$ in (5-11m). Moreover, through (5-11n) we constrain $\theta_{\cdot,\omega}$ values in the model to a neighborhood of the observed values. This is done to reduce out–of–sample errors.

6
Case Studies

This section presents numerical results to illustrate the performance of the proposed EDC–NR. We run two different kinds of tests. The first one, fully described in Section 6.2, is a controlled test, where we create load scenarios by sorting loads values assuming that they follow normal distributions. Then, the optimal generation dispatch for each scenario is determined. For these created operating points, we use the EDC–NR to estimate parameters of the EDCPF model. At last, a performance analysis compares the EDCPF with a Ward reduced model. The second test, described in Section 6.3, differs from the first concerning the load profile used. In this case, we consider that loads vary following a pattern dictated by a real load pattern originated from a Brazilian distribution company.

In this work, Ward reduction was performed using Organon software [46]. All developed programming were implemented in Julia [47] using PowerModels [48] and JuMP [49] packages for power systems and optimization problems modeling.

6.1
Accuracy Metric

In this section we formulate the error metric that we use to evaluate the performance of a reduced network. It compares the results of the base system and the reduced one in relation to some PF variables. In the cases presented in this work, even though the variables of interest are the power flow in the selected lines and the total power lost, we evaluate performance only through the selected lines PF, while the base system is the complete network AC PF model.

The metric used is defined as the worse power flow estimation error among all selected lines in a given scenario. It is calculated following a few steps. First, we compute the power flow in each selected branch for both complete ($f_{(k,m),\omega}^{\text{complete}}$) and reduced systems($f_{(k,m),\omega}^{\text{reduced}}$). Then, we calculate the selected lines PF estimation errors $\delta f_{(k,m),\omega}$, which are the absolute values of the difference between $f_{(k,m),\omega}^{\text{complete}}$ and $f_{(k,m),\omega}^{\text{reduced}}$ in relation to their transmission capacity $\overline{F}_{(k,m)}$. Finally, our error metric for a given scenario (δf_{ω}) is the worse

of these errors for that scenario, hereinafter, simply referred to as the error. It is mathematically defined as follows:

$$\delta f_{(k,m),\omega} = \left| \frac{f^{\text{complete}}_{(k,m),\omega} - f^{\text{reduced}}_{(k,m),\omega}}{\overline{F}_{(k,m)}} \right| \qquad \forall \, (k,m) \in \mathcal{L}^S, \, \omega \in \Omega \qquad \text{(6-1a)}$$

$$\delta f_{\omega} = \max_{(k,m)\in\mathcal{L}^S} \{\delta f_{(k,m),\omega}\} \qquad \forall \, \omega \in \Omega \qquad \text{(6-1b)}$$

By computing the error δf_{ω} for a set of relevant scenarios, interesting statistical analysis can be performed to observe the behavior and tendency of the reduced network. In this peace of work, we are constantly plotting and comparing the error histograms for Ward and proposed EDCPF reduced networks together with their average and maximum errors.

6.2
Controlled Cases

In this set of tests, we evaluate two EDCPF responses, one for the IEEE 24-Bus test system and the other for the IEEE 118-Bus test system. For these tests, we want to control the load profile variation. These two system base cases are presented in [50].

We simulate a set of scenarios to evaluate the methodology. Here, a scenario is defined as the collection of selected branches PFs and the boundary bus voltage angles for a specific load and generation profile. In the studies presented in this section, all scenarios were obtained from AC OPF simulations considering controlled load values. We assume that loads (active and reactive components) follow normal distributions of this format:

$$P_k^D \sim \mathcal{N}(P_{k,0}^D, \, P_{k,0}^D \, \sigma_{\text{in}}) \qquad \forall k \in \mathcal{B} \qquad \text{(6-2a)}$$

$$Q_k^D \sim \mathcal{N}(Q_{k,0}^D, \, Q_{k,0}^D \, \sigma_{\text{in}}) \qquad \forall k \in \mathcal{B} \qquad \text{(6-2b)}$$

where $\mathcal{B}$ is the set of all system buses. $P_{k,0}^D$ and $Q_{k,0}^D$ are bus k active and reactive demand in the base case. Therefore, the noise σ_{in} defines the distribution standard deviation as a fraction of the base case complex demand. In this manner, by varying σ_{in}, we can control the range of operating points in our set of scenarios. The following algorithm clarifies the process used to simulate

N_{in} scenarios.

Algorithm 1: Scenarios Simulation

Result: $\boldsymbol{\xi}^{\text{obs}}$, $\boldsymbol{y}^{\text{obs}}$

Inputs: $\boldsymbol{P_0^D}$, $\boldsymbol{Q_0^D}$, σ_{in}, N_{in}

for $\omega = 1 : N_{in}$ **do**

    for $k \in \mathcal{B}$ **do**

        Draw a value for $P_{k,\omega}^D$ assuming $P_k^D \sim \mathcal{N}(P_{k,0}^D, \, P_{k,0}^D \sigma_{\text{in}})$;

        Store $P_{k,\omega}^D$ in $\boldsymbol{\xi}_\omega$

        Draw a value for $Q_{k,\omega}^D$ assuming $Q_k^D \sim \mathcal{N}(Q_{k,0}^D, \, Q_{k,0}^D \sigma_{\text{in}})$;

        Store $Q_{k,\omega}^D$ in $\boldsymbol{\xi}_\omega$

    end

    Run AC OPF considering the loads in $\boldsymbol{\xi}_\omega$;

    Store $\Theta_{k,\omega}$, $P_{k,\omega}^G$ $\forall k \in \mathcal{B}$ in $\boldsymbol{\xi}_\omega$;

    Store P_ω^{loss} and $F_{(k,m),\omega}$ $\forall (k,m) \in \mathcal{L}^S$ in $\boldsymbol{y}^{\text{obs}}$.

end

6.2.1
IEEE 24–Bus System Results

In this study, the IEEE 24–Bus test system is partitioned into an external system, boundary, and internal system, as indicated in Figure 6.1(a). Additionally, we consider all preserved power lines as selected lines ($\mathcal{L}^S \equiv \mathcal{L}^I \cup \mathcal{L}^B$). Thus, we perform a comparative analysis between the equivalent reduced system obtained with the Ward method applied to the nominal load profile of the base case (described in [50]), and the EDCPF reduced network equivalent model obtained with our proposed method. The comparison is based on metric (6-1b) for the selected lines active PF.
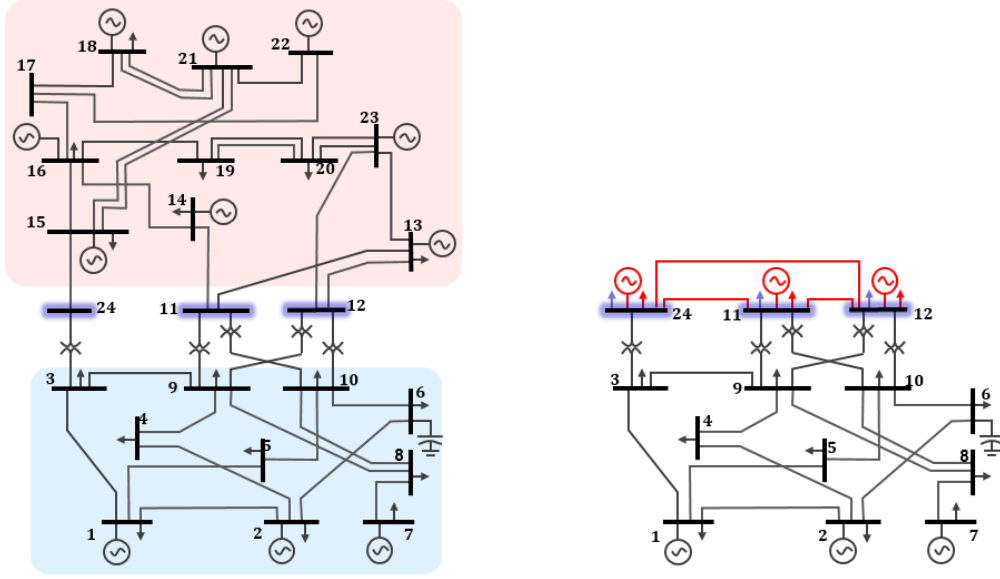
6.1(a): IEEE 24-Bus test system where 1–10 are internal buses; 11, 12 and 24 are boundary buses; and 13–23 are external buses.

6.1(b): Reduced 24–Bus test system scheme.

Figure 6.1: IEEE 24–Bus test system partition scheme.

The performance analysis is given as follows. For each run of our EDC–NR model, we consider N_{in} scenarios (simulated as indicated in Algorithm 1) to obtain the EDCPF reduced model. Then, we evaluate the error metric for both the Ward and our proposed method for others N_{out} simulated scenarios (out–of–sample). We repeat this process for N_σ different values of input noise σ_{in} to evaluate its effect in the average and worse errors of the reduced methods.

Algorithm 3 demonstrates the steps of the performance analysis. Input $\sigma_{in,1}$ is the noise σ_{in} of the first analysis; $\Delta\sigma_{in}$ is the step between each σ_{in} analysis noise; λ and α_θ are constants of the EDC–NR model; N_σ is the number of analysis performed per network equivalent; N_{in} and N_{out} respectively are the number of scenarios considered in the EDC–NR model and in the out–of–sample analysis. The results of the performance analysis are the vector $\boldsymbol{\sigma}_{in}$ that stacks all analysis σ_{in}; Vectors $\boldsymbol{E}_\epsilon^{\text{Ward}}$ and $\boldsymbol{M}_\epsilon^{\text{Ward}}$, which respectively stacks all Ward performance analyses average and worse errors; Vectors $\boldsymbol{E}_\epsilon^{\text{EDCPF}}$ and $\boldsymbol{M}_\epsilon^{\text{EDCPF}}$, which respectively stacks all EDCPF performance analyses average and worse errors.

In this study, the inputs considered were:

$$(\sigma_{in,1}, \Delta\sigma_{in}, \lambda, \alpha_\theta, N_{pc}, N_p, N_\sigma, N_{in}, N_{out}) =$$

$$(10^{-6}, 0.005, 0.6, 0.25, 5, 2, 11, 400, 2000) \quad (6\text{-}3)$$

where parameters λ and α_θ were empirically chosen by experimentation. For mismatch loss functions, we chose to use a polynomial order $N_p = 2$ to avoid poor out–of–sample performance. The number of principal components N_{PC} to consider depends on the computational processing capacity of the machine used to solve the EDC–NR problem since the number of decision variables increases with N_{PC}. For this reason we considered $N_{PC} = 5$ for this 24–Bus system.

Algorithm 2: Performance Analysis

Result: $\boldsymbol{\sigma}_{\text{in}}$, $\boldsymbol{E}_\epsilon^{\text{Ward}}$, $\boldsymbol{M}_\epsilon^{\text{Ward}}$, $\boldsymbol{E}_\epsilon^{\text{EDCPF}}$, $\boldsymbol{M}_\epsilon^{\text{EDCPF}}$

Inputs: $\sigma_{\text{in},1}$, $\Delta\sigma_{\text{in}}$, λ, α_θ, N_σ, N_{pc}, N_p, N_{in}, N_{out}

Create a Ward reduced network

for $i = 1 : N_\sigma$ **do**

    Simulate N_{in} scenarios as indicated by Algorithm 1 for $\sigma_{\text{in},i}$;

    Define $\boldsymbol{x}_i$ by Solving the EDC–NR model (Equation (5-11)) considering λ, α_θ, N_{pc}, N_p and the N_{in} simulated scenarios;

    for $j = 1 : N_{out}$ **do**

        Simulate scenario $\boldsymbol{\xi}_j$ considering $\sigma_{\text{in},i}$;

        Solve the complete system AC PF for $\boldsymbol{\xi}_j$ (Equation (2-1));

        Solve the $\hat{\boldsymbol{y}}^{\text{EDCPF}}(\boldsymbol{x}_i, \xi_j)$ (Equaiton (5-9));

        Calculate $\delta f_j^{\text{EDCPF}}$ for the EDCPF$_i$ for $\boldsymbol{\xi}_j$ (Equation (6-1));

        Solve the Ward reduced system ACPF for $\boldsymbol{\xi}_j$ (2-1));

        Calculate δf_j^{Ward} for the Ward reduction for $\boldsymbol{\xi}_j$ (Equation (6-1));

        Store $\delta f_j^{\text{EDCPF}}$ and δf_j^{Ward} at $\boldsymbol{\Delta f}_i^{\text{EDCPF}}$ and $\boldsymbol{\Delta f}_i^{\text{Ward}}$;

    end

    Store $\mathbb{E}\left[\boldsymbol{\Delta f}_i^{\text{EDCPF}}\right]$ in $\boldsymbol{E}_\epsilon^{\text{EDCPF}}$;

    Store $\max\left\{\boldsymbol{\Delta f}_i^{\text{EDCPF}}\right\}$ in $\boldsymbol{M}_\epsilon^{\text{EDCPF}}$;

    Store $\mathbb{E}\left[\boldsymbol{\Delta f}_i^{\text{Ward}}\right]$ in $\boldsymbol{E}_\epsilon^{\text{Ward}}$;

    Store $\max\left\{\boldsymbol{\Delta f}_i^{\text{Ward}}\right\}$ in $\boldsymbol{M}_\epsilon^{\text{Ward}}$;

    Store $\sigma_{\text{in},i}$ in $\boldsymbol{\sigma}_{\text{in}}$;

    $\sigma_{\text{in},i+1} = \sigma_{\text{in},i} + \Delta\sigma_{\text{in}}$;

end

Plot $\boldsymbol{\sigma}_{\text{in}}$ versus $\boldsymbol{E}_\epsilon^{\text{Ward}}$ and $\boldsymbol{M}_\epsilon^{\text{Ward}}$;

Plot $\boldsymbol{\sigma}_{\text{in}}$ versus $\boldsymbol{E}_\epsilon^{\text{EDCPF}}$ and $\boldsymbol{M}_\epsilon^{\text{EDCPF}}$.

At the end of the performance analysis, we plot the graphics in Figure 6.2. It shows how the average and worse error of both Ward and EDCPF reduced models varies according to the noise σ_{in}. We observe that for small values of σ_{in}, Ward ACPF presents lower errors. This response is expected as the Ward model is exact at the base case, which occurs for $\sigma_{\text{in}} = 0$. For instance, as the EDCPF is a linearized approximation, it will present some errors inherent to it. To illustrate this feature, Figure 6.3 shows the error histogram for $\sigma_{\text{in}} = 0.01$, where Ward reduction outperforms the EDCPF Further, as σ_{in} increases, we

can observe how Ward model loses precision while the EDCPF keeps a relative stable performance. Figure 6.4 shows the error histogram for $\sigma_{in} = 0.03$.
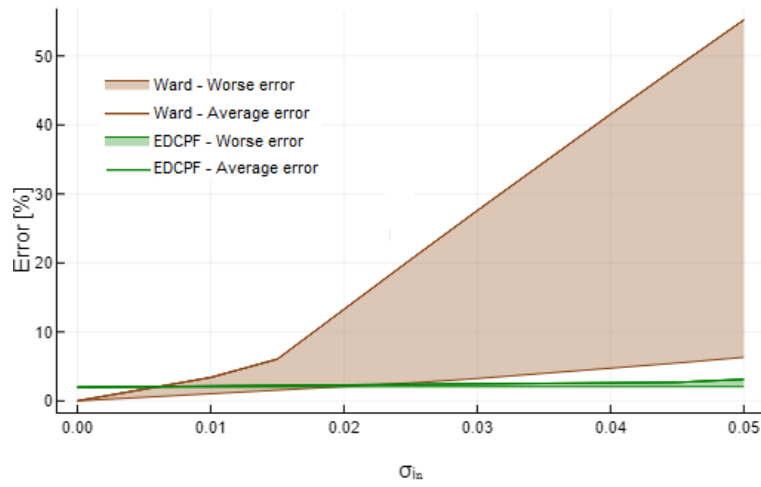

Figure 6.2: EDCPF and Ward performance for the 24–Bus system when σ_{in} varies.
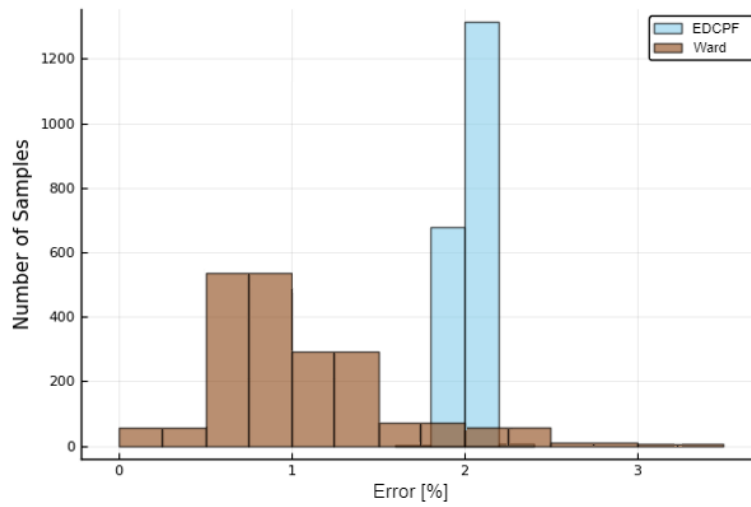

Figure 6.3: EDCPF and Ward error histogram for the 24–Bus system for $\sigma_{in} = 0.01$.
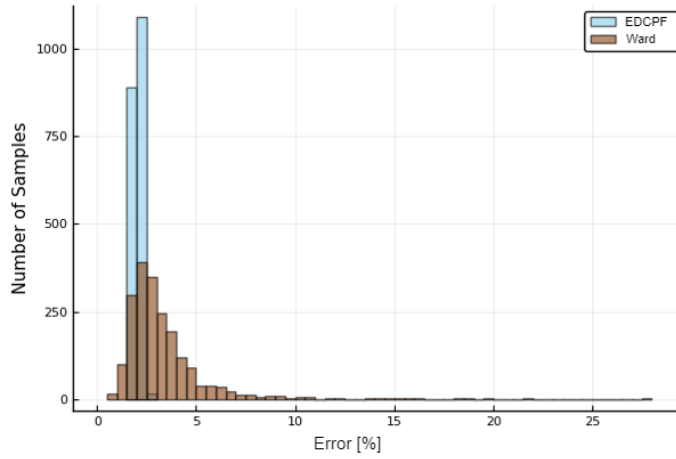
Figure 6.4: EDCPF and Ward error histogram for the 24–Bus system for $\sigma_{\text{in}} = 0.03$.

6.2.2
IEEE 118–Bus System Results

In this study, we repeat the same steps of Section 6.2.1 but for the IEEE 118–Bus test system. The electrical diagram of the system with the external area and boundary identification is presented in Figure 6.4. Note that in this case, the two subsystems that form the external area are not directly interconnected. The test system and its areas description are described in reference [50]. As in Section 6.2.1, all power lines from the study area are considered selected lines ($\mathcal{L}^S \equiv \mathcal{L}^I \cup \mathcal{L}^B$).
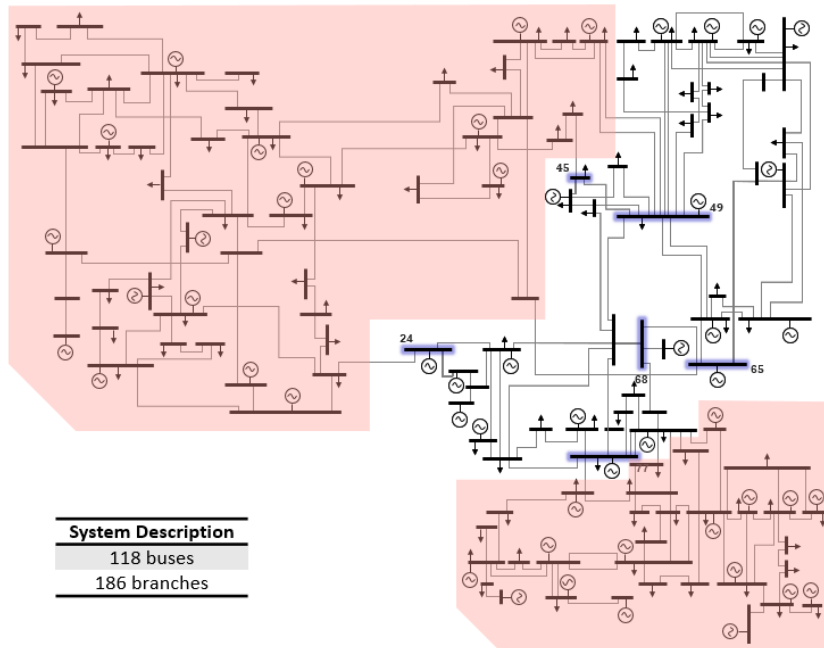
6.5(a): IEEE 118–Bus test system partition scheme. Boundary bus defined and external system identified.
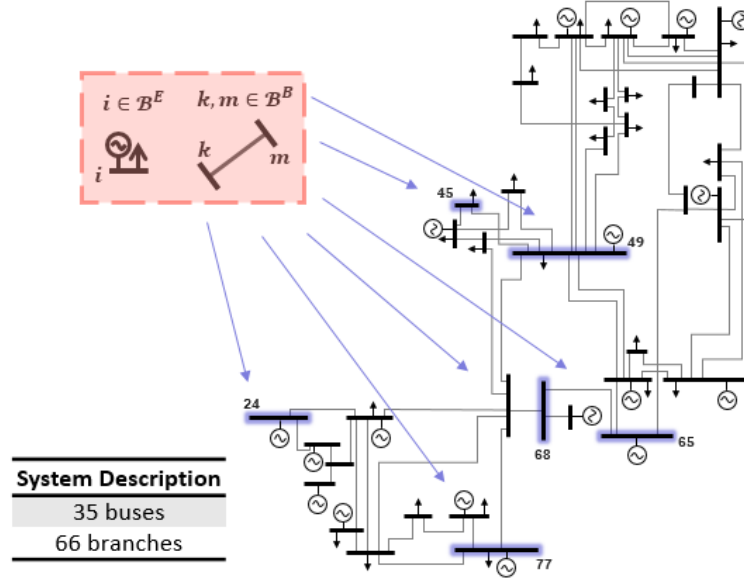
6.5(b): Reduced 118–Bus test system scheme.

Figure 6.4: IEEE 118–Bus test system partition scheme.

For the EDC-NR model, we considered 400 simulated samples and for each performance analysis, we considered 1000 samples. As in the 24–Bus system, $\lambda = 0.8$ and $\alpha = 0.3$ were empirically chosen. We also use $N_p = 2$ to benefit from quadratic properties and $N_{\text{PC}} = 40$ to represent great part of the loads variances. In short, the inputs considered in Algorithm 3 were:

$$(\sigma_{\text{in},1}, \Delta\sigma_{\text{in}}, \lambda, \alpha_\theta, N_{\text{pc}}, N_p, N_\sigma, N_{\text{in}}, N_{\text{out}}) =$$
$$(10^{-6}, 0.001, 0.8, 0.3, 40, 2, 21, 400, 1000) \quad (6\text{-}4)$$

Thus, Figure 6.5 shows the performance analysis results. Once again we can testify how the Ward reduction presents better results when loads of the system are close to the base system. Additionally, when the noise σ_{in} and load values dispel from the base case, the EDCPF keeps very low error in comparison to the ward reduced system.

Figure 6.5: EDCPF and Ward performance for the 118–Bus system when σ_{in} varies.

Figure 6.6: EDCPF and Ward error histogram for the 118–Bus system for $\sigma_{\text{in}} = 0.005$.

Figure 6.7: EDCPF and Ward error histogram for the 24–Bus system for $\sigma_{\text{in}} = 0.06$.
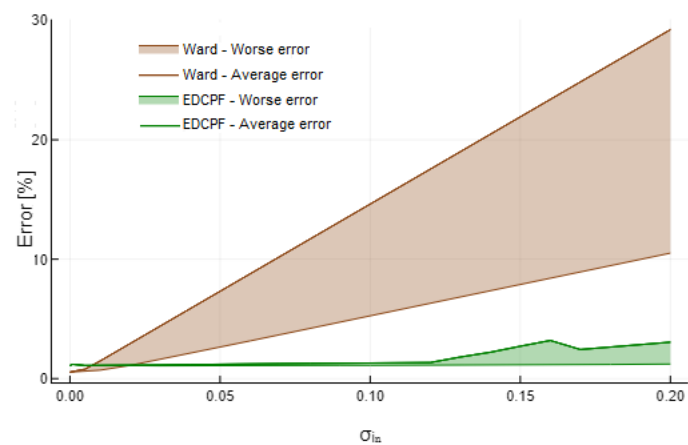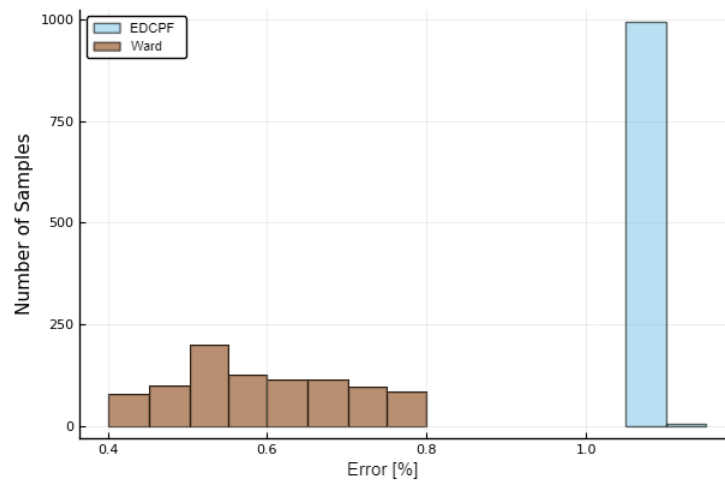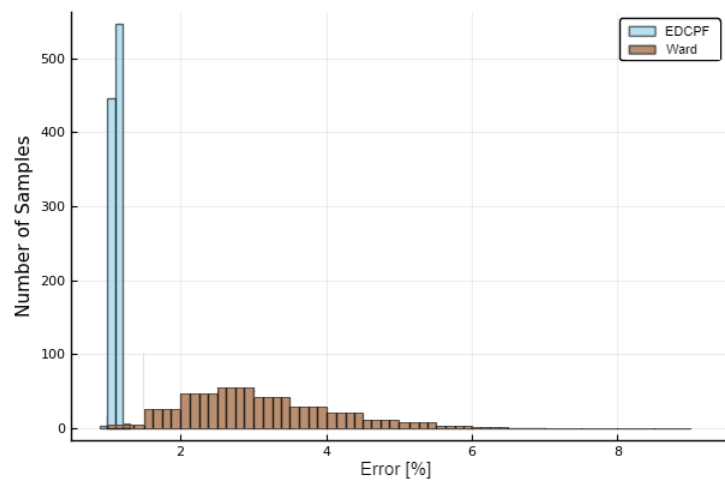
6.3
Realistic Cases

This study has as main objective to evaluate the performance of the proposed reduced network in more realistic scenarios. The case studies of Section 6.2 have the fundamental importance of showing the robustness of the proposed method to changes in the operative condition of a power system. However, these synthetic scenarios are non-realistic since they assume that active and reactive loads follow uncorrelated normal distributions. In actual real power systems, loads behavior are correlated and present seasonal variations. In this manner, to complement our analysis regarding the EDC–NR, we include a study where we investigate the performance of both, EDCPF and Ward reduced models, for the IEEE 118–Bus test system when some loads follow a typical pattern.

The study consists of two performance analysis. In the first, we will consider that one internal load of the 118–Bus system has a realistic seasonal tendency and all other loads are constant. Then, we compare Ward and EDCPF performance. In the second analysis, we will consider that all 25 internal loads of the test system varies according to realistic tendencies while external loads are fixed. Thus, we compare Ward and EDCPF for this case as well. The reason for keeping external loads fixed is that it is in our interest to evaluate performance in situations where Ward reduced systems can deliver their best results. Since Ward reduction can not interpret external system variations, the best results are for constant external loads.

The realistic tendencies were extracted from real readings of a Brazilian distribution company. Specifically, these readings consist of 25 pairs of active and reactive load time series, sampled on an hourly basis for the period of almost one year (8200 samples). We proceeded in the following manner to replicate these series in the internal loads of the IEEE 118-Bus test system. First, we normalized the series by their maximum values (Figure 6.7 shows three pairs of these series). Then, we randomly associate each of the 25 normalized pairs of series to one of the 118–Bus system internal load. Thus, we rescale the series by their associated load base values. With that, we have the 25 pairs of active and reactive load series, one for each internal system load, presented in [50].

In the examples of Section 6.2, we considered that loads followed normal distributions. Thus, we could generate the scenarios used in the EDC–NR models and the performance analysis. However, in this Section's case studies, for the loads with real tendency, its associated load series empirically determines its load distribution. All other system loads are deterministic, fixed to the base

case values. With that, we can generate scenarios through AC OPFs, which defines generation dispatches and all other observations that compound the scenarios. Note that for each case study we are limited to 8200 scenarios, one for each instant of time represented in the loads series.

In the following studies, we constantly select a number n of scenarios to analyze. To generate them, we always collect n samples of the system load series and perform the OPF for them. The load samples are equally spaced in time, covering the whole range of the series.
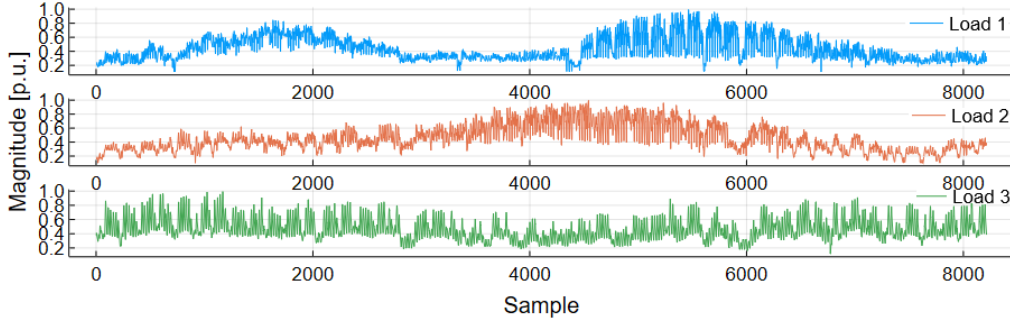
6.8(a): Loads active component.
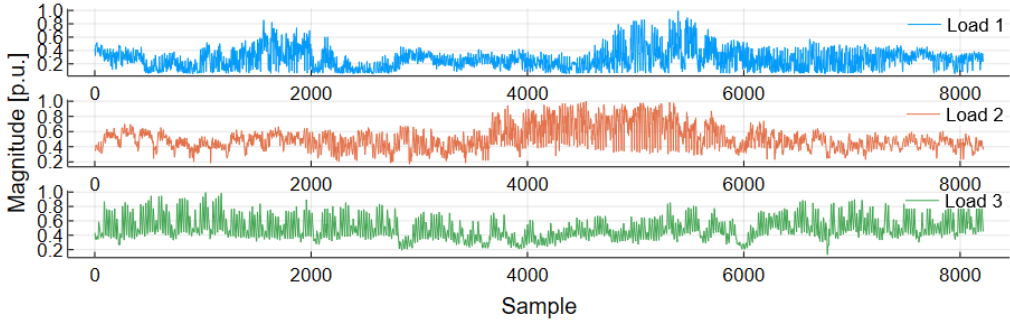
6.8(b): Loads reactive component.

Figure 6.7: 3 normalized load time series.

For the sake of fairness, before running the two performance analysis, we run a preliminary test to define which bus should be the reduced system slack bus. We want it to be at the boundary bus that gives the best performance for the Ward equivalent. For that, we run six short performance analysis, one per boundary bus as a slack bus. For each one of these six tests, we create 50 from the 8200 possible scenarios. Then, we evaluate Ward's performance for these scenarios and record the average error. Table 6.3 summarizes the results and indicates that bus 77 must be the slack bus since it shows better performance.

Finally, we can perform the two realistic analyses, one with only one varying load and another with all internal loads varying. For training the

Slack bus	Average Error	
	1 variable load	25 variable loads
24	1.55%	43.9%
45	2.72%	82.0%
49	2.08%	13.3%
65	0.75%	12.8%
68	0.88%	12.4%
77	0.58%	11.0%

Table 6.1: Ward performance per slack bus

EDC–NR model we chose the following parameters:

$$(\lambda, \, \alpha_\Theta, \, N_p, N_{\text{in}}) = (0.5, \, 0.35, \, 2, \, 300) \tag{6-5}$$

where λ, α_Θ and N_{PC} were defined by experimentation. In relation to the two studies Ward reduced networks, They were created based in the case with the greater total peak active load in their set of 300 input scenarios.

For the case with one varying internal load we only need to consider one principal component ($N_{\text{PC}} = 1$) and we evaluate performance considering 1500 scenarios. As result, Figure 6.8 shows the error histogram for both, EDCPF and Ward reduced network. We can notice that Ward equivalent presents reduced average error in comparison to the EDCPF. This is justified by the fact that in this case, as only one load of the system varies, we have scenarios with operating conditions close to the base case in which Ward model was derived.
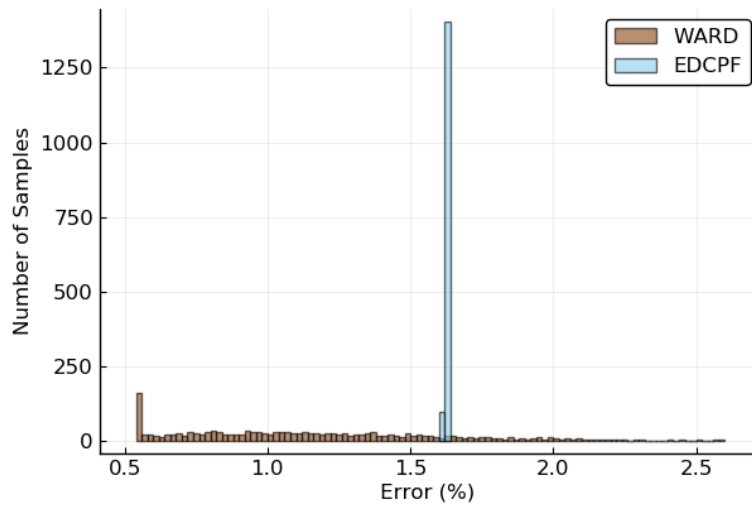
Figure 6.8: EDCPF and Ward error histogram for the case where only one internal load changes.

We considered 1500 scenarios for the second case where all 25 internal

loads have a realistic profile, as well. In this experiment, we established that the principal components should recover at least 90% of the system loads variance. Thus, we set $N_{\text{PC}} = 7$, representing 91.2% of the variation. Figure 6.9 shows the error histogram of both EDCPF and ward reduced AC PF. From that, we infer that the proposed model presents minor average error and deviation. This result goes with Section 6.2 results where the EDCPF was shown to be more precise for operating points distant to the base case. In relation to computational performance, the proposed reduced linear method had an average solving time equal to 11.5% of the original system AC PF average time. Ward AC PF average solving time was equal to 33.6% of AC PF time. Regarding the network reduction, both cases eliminated 82 buses. They also decreased the number of branches from 186 to 66.
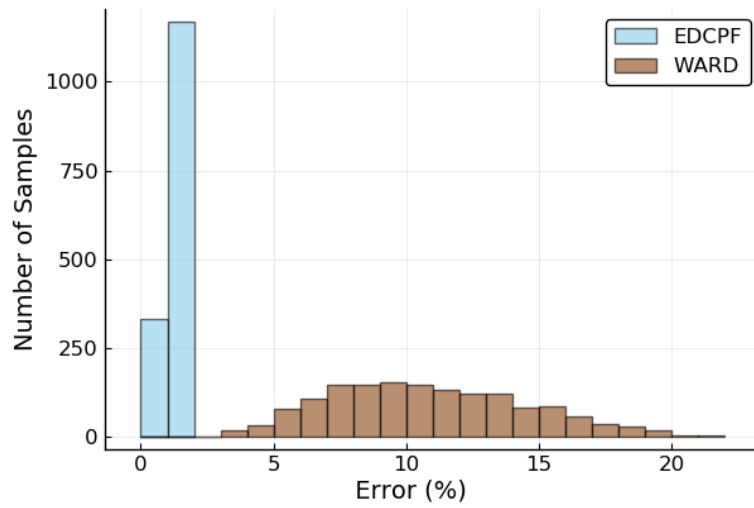

Figure 6.9: EDCPF and Ward error histogram for the case where all internal loads changes.

7
Conclusion

In this work, we proposed a general method to estimate the parameters of PF equivalent models. The framework is used to build a novel reduced linear PF model identified as EDCPF. For that, we reshape the general structure as a linear optimization problem named EDC–NR, which considers multiple operating scenarios as input. Specifically, EDC–NR objective function is the minimization of average errors between observed power flows and the response of the EDCPF. The proposed enhanced-dc equivalent model is defined by: 1) the allocation of each external generator injection and load extraction to a given set of boundary buses; 2) the determination of new lines connecting pairs of boundary buses (equivalent for the external system); and 3) the coefficients of polynomial functions that permits to include the network losses into the DC model. In summary, the EDC–NR can be seen as a learning regression model that retains the linearity of DC PF models while approximating the response to observed data employing polynomial loss function.

In this work, the EDC–NR and the EDCPF walk together in the sense that the EDC–NR is proved to be efficient by the results of the EDCPF model estimated through it. Study cases considering both, IEEE 24–Bus and IEEE 118–Bus test systems with totally controlled scenarios and scenarios with realistic load profiles strongly suggest the following:

– The EDC–NR considering great number of scenarios can derive EDCPF models that generally outperforms the classical Ward reduction in terms of average and maximum deviation accuracy.

– The use of the proposed EDC-NR greatly minimizes the risks when employing reduced networks. In realistic situations where the system operating point is constantly changing, it shows a very small standard deviation in comparison with the Ward model

– Solving an AC PF in Ward reduced systems takes more time than solving the EDCPF problem. In some simulations, Ward gets to be 200% slower on average.

We conclude that the EDC–NR together with the EDCPF fulfill our expectations. The EDCPF is a reduced linear power flow model, therefore pre-

senting reduced solving time, that shows more precise load flow response than the most traditional method in the literature. We believe that the proposed EDC–NR can strongly benefits from this optimization network resulting in even better EDCPF models. In an upper level, we encourage the application of the proposed method in larger power systems and the development of new reduced models, especially for OPF studies, with parameters defined by the general framework of (4-1). Future works are listed below.

– Realization of new tests regarding the proposed models considering more complex power systems in realistic load scenarios. These tests are important to evaluate how the EDC–NR behave when the problem grows in relation to its sets of constraints and variable dimensions.

– Study PCA use in systems with an increased number of loads to better evaluate its true benefits and limitations.

– Study the effects of considering buffer zones or the retention of other external structures.

A
Nomenclature

This section presents the nomenclature and symbols used in this work. Note the in cases where we are treating with one specific scenario, the subscript ω may be omitted.

Sets and Indices

$\mathcal{B}$	Set of all system bus indices k
$\mathcal{B}^E$	Set of external bus indices i
$\mathcal{B}^B$	Set of boundary bus indices j
$\mathcal{B}^I$	Set of internal bus indices k
$\mathcal{B}^{\mathbf{REF}}$	Set of reference bus indices k
$\mathcal{L}$	Set of all pairs of buses indices (k, m) that branches connections.
$\mathcal{L}^B$	Set of pairs of buses indices (k, m) defining branches connecting internal and boundary buses (boundary lines)
$\mathcal{L}^I$	Set of pairs of buses indices (k, m) defining branches connecting internal buses (internal lines)
$\mathcal{L}^S$	Set of pairs of buses indices (k, m) defining branches connecting selected line indices
$\mathcal{L}^N$	Set of pairs of buses indices (k, m) defining new lines
Ω	Set of scenario indices ω

Functions

$\hat{\mathbf{y}}(\cdot)$	Function that predicts power flow variables of interest
$\rho(\cdot)$	Norm based function

Constants

$A_{(k,m),\omega}$	Tap of the transformer from bus k to bus m in scenario ω
$\Phi_{(k,m),\omega}$	Shift angle of the transformer from bus k to bus m in scenario ω
$R_{(k,m)}$	Branch (k,m) series resistance
$X_{(k,m)}$	Branch (k,m) series reactance.
$G_{(k,m)}$	Branch (k,m) series conductance
$B_{(k,m)}$	Branch (k,m) series susceptance
$B_{(k,m)}^{\mathbf{sh}}$	Line (k,m) model–π shunt susceptance
$B_k^{\mathbf{sh}}$	Bus k shunt susceptance
$\overline{F}_{(k,m)}$	Branch (k,m) power flow limit
P_k^D	Bus k active load
Q_k^D	Bus k reactive load
$\overline{P}_k$	Bus k active generation upper limit
$\underline{P}_k$	Bus k active generation lower limit
$\overline{Q}_k$	Bus k reactive generation upper limit
$\underline{Q}_k$	Bus k reactive generation lower limit
$\overline{V}_k$	Bus k voltage magnitude upper limit
$\underline{V}_k$	Bus k voltage magnitude lower limit
$\mathbf{Y}$	Nodal admittance matrix
$\mathbf{V}$	Column vector that stacks all nodal complex voltages
$\mathbf{J}$	Column vector that stacks all nodal current injection
$\mathbf{Y_{EE}}$	External system nodal admittance submatrix
$\mathbf{Y_{BB}}$	Boundary nodal admittance submatrix
$\mathbf{Y_{II}}$	Internal system nodal admittance submatrix
$\mathbf{Y_{EB}}$	Admittance submatrix of the branches connecting external system and boundary

$\boldsymbol{Y}_{\mathbf{BE}}$ Admittance submatrix of the branches connecting boundary and external system

$\boldsymbol{Y}_{\mathbf{BI}}$ Admittance submatrix of the branches connecting boundary and Internal system

$\boldsymbol{Y}_{\mathbf{IB}}$ Admittance submatrix of the branches connecting internal system and boundary

$\boldsymbol{V}_{\mathbf{E}}$ Column vector that stacks External system complex voltages

$\boldsymbol{V}_{\mathbf{B}}$ Column vector that stacks boundary complex voltages

$\boldsymbol{V}_{\mathbf{I}}$ Column vector that stacks internal system complex voltages

$\boldsymbol{J}_{\mathbf{E}}$ Column vector that stacks External system nodal current injection

$\boldsymbol{J}_{\mathbf{B}}$ Column vector that stacks boundary nodal current injection

$\boldsymbol{J}_{\mathbf{I}}$ Column vector that stacks internal system nodal current injection

$\mathbf{Y}_{\mathbf{BB}}^{eq}$ External equivalent nodal admittance submatrix

$\boldsymbol{J}_{\mathbf{B}}^{eq}$ Column vector that stacks boundary equivalent current injection

π_{ω} Weigh of the ω parcel of the expected value of $\rho(\boldsymbol{\varepsilon}_{\omega})$

$\mathbf{y}_{\omega}^{obs}$ Vector that stacks all observed power flow variables of interest in scenario ω

ξ_{ω}^{obs} Vector that stacks all the observed data defining a scenario ω

$D_{k,\omega}^{\mathbf{PC}}$ kth principal component of scenario ω load vector

N_p Mismatch polynomial functions order

$N_{\mathbf{PC}}$ Number of considered principal components

λ Constant that defines the linear combination regarding load flow and total loss estimation errors

$P_{\omega}^{\mathbf{loss}}$ Observed total power loss in scenario ω

$\boldsymbol{F}_{\omega}^{S}$ Vector that stacks all selected lines observed active power flow in scenario ω

$F_{(k,m),\omega}$ Line (k,m) observed active power flow in scenario ω

$\Theta_{j,\omega}$ Bus j observed voltage angle in scenario ω

α_θ Fraction of $\Theta_{j,\cdot}$ used to constrain $\theta_{j,\cdot}$ for all $j \in \mathcal{B}^B$

$f_{(k,m),\omega}^{\mathbf{complete}}$ complete system active power flow in line (k,m) for scenario ω

$f_{(k,m),\omega}^{\mathbf{reduced}}$ Reduced system active power flow in line (k,m) for scenario ω

$\delta f_{(k,m),\omega}$ Absolute value of the difference between $f_{(k,m),\omega}^{\mathrm{true}}$ and $f_{(k,m),\omega}^{\mathrm{reduced}}$ normalized by line (k,m) power limit.

δf_ω Worse $\delta f_{(k,m),\omega}$ between all scenarios

$\sigma_{\mathbf{in}}$ Input noise in the set of load scenarios

$P_{k,0}^D$ Base case actove power demand at bus k

$Q_{k,0}^D$ Base case reactove power demand at bus k

$\boldsymbol{P}_0^D$ Vector that stacks all base case active power demands

$\boldsymbol{P}_0^Q$ Vector that stacks all base case reactive power demands

Variables

$v_{k,\omega}$ Bus k voltage angle in scenario ω

$\theta_{k,\omega}$ Bus k voltage angle in scenario ω

$p_{(k,m),\omega}$ Branch (k,m) active power flow in scenario ω

$q_{(k,m),\omega}$ Branch (k,m) reactive power flow in scenario ω

$f_{(k,m),\omega}$ Branch (k,m) apparent power flow in scenario ω

$p_{k,\omega}^G$ Active generation at bus k in scenario ω

$q_{k,\omega}^G$ Reactive generation at bus k in scenario ω

$p_{j,\omega}^{\mathbf{loss}}$ Active generation at bus j in scenario ω

$\boldsymbol{\varepsilon}_\omega$ Vector that stacks all difference between observed and predicted power flow variables of interest for scenario ω

$\boldsymbol{x}$ Vector that stacks all reduced network parameters, $x_{(k,m)}^B$, $x_{i,j}^G$, $x_{i,j}^D$ and $x_{j,n,k}^{\mathrm{loss}}$

$x_{(k,m)}^B$ Susceptance of new line (k,m) connecting boundary buses

$x_{i,j}^{G}$ Fraction of bus i active generation that must be allocated at boundary bus j

$x_{i,j}^{D}$ Fraction of bus i active load that must be allocated at boundary bus j

$x_{j,n,k}^{\textbf{loss}}$ Coefficients of the polynomial functions of principal component k which describes the part of total power loss allocated at bus j

$f_{(k,m),\omega}^{N}$ New line (k,m) active power flow in scenario ω

$p_{j,\omega}^{D}$ Active load at bus j in scenario ω

$p_{j,\omega}^{\textbf{loss}}$ Part of system total active loss allocated at bus j in scenario ω

$\boldsymbol{\varepsilon}_{\omega}^{F}$ Vector that stacks all difference between observed and predicted selected lines load flow variables of interest in scenario ω

$\varepsilon_{(k,m),\omega}^{\textbf{loss}}$ Difference between the observed and the predicted total power loss at scenario ω

$\delta_{\omega}^{\textbf{loss}}$ Absolute value of the difference between the observed and the predicted total power loss at scenario ω

$\delta_{(k,m),\omega}^{F}$ Absolute value of the difference between the observed and the reduced system active flow in branch (k,m) at scenario ω

B
Principal Component Analysis

This appendix presents the basic ideas behind the PCA applied in this work. It summarizes important information described in [51, 52].

The focus in PCA is to represent a set of correlated data as a reduced set of equivalent uncorrelated variables called principal components (PC). Here, first, we will introduce the concept of PC when the objective is to transform a vector of p random variables. Secondly, we expand the concept to the case where we deal with samples of random variables populations.

B.1
Population Principal Components

The principal components of a vector with random variables $\boldsymbol{x} = (x_1, x_2, \ldots, x_p)'$ has it elements defined by:

$$\boldsymbol{z}_k = \boldsymbol{\alpha}_k' \boldsymbol{x} = \sum_{j=1}^{p} \alpha_{kj} x_j \tag{B-1}$$

$$\boldsymbol{\alpha}_k = (\alpha_{k1}, \alpha_{k2}, \ldots, \alpha_{kp})' \tag{B-2}$$

where $\boldsymbol{\alpha}_k$ is the vector of weights that maximizes the variance of the PC z_k. Therefore, its elements are determined as follow:

$$\boldsymbol{\alpha}_k \in \operatorname*{argmax}_{\boldsymbol{\alpha}_k} \quad \mathrm{Var}[\boldsymbol{\alpha}_k' \boldsymbol{x}] \tag{B-3a}$$

$$\text{s.t:} \quad \boldsymbol{\alpha}_k' \boldsymbol{\alpha}_k = 1 \tag{B-3b}$$

note that without constraint (B-3b), the solution of the optimization problem in (B-3a) would be when the elements of $\boldsymbol{\alpha}_k$ are set to infinity. Therefore it is a normalization constraint to guarantee limited elements for $\boldsymbol{\alpha}_k$ establishing $\boldsymbol{z}_k$ as a linear combination of the elements of $\boldsymbol{x}$.

The variance of a linear combination as $\mathrm{Var}[\boldsymbol{\alpha}_k' \boldsymbol{x}]$ is equal to $\boldsymbol{\alpha}_k' \boldsymbol{\Sigma} \boldsymbol{\alpha}_k$, where $\boldsymbol{\Sigma}$ is the covariance matrix of $\boldsymbol{x}$. In this manner, by recurring to Lagrange multipliers we can solve problem (B-3) as:

$$L(\lambda) = \boldsymbol{\alpha}_k' \boldsymbol{\Sigma} \boldsymbol{\alpha}_k - \lambda(\boldsymbol{\alpha}_k' \boldsymbol{\alpha}_k - 1) \tag{B-4a}$$

$$\frac{\partial L}{\partial \lambda} = \lambda(\boldsymbol{\alpha}'_k \boldsymbol{\alpha}_k - 1) = 0 \tag{B-4b}$$

$$\frac{\partial L}{\partial \boldsymbol{\alpha}_k} = \boldsymbol{\Sigma} \boldsymbol{\alpha}_k - \lambda \boldsymbol{\alpha}_k = 0 \tag{B-4c}$$

where Equation (B-4c) can be reformulated to

$$(\boldsymbol{\Sigma} - \lambda \boldsymbol{I}_p)\boldsymbol{\alpha}_k = 0 \tag{B-5}$$

By definition, λ and $\boldsymbol{\alpha}_k$ are eigenvalue and eigenvector for the covariance matrix $\boldsymbol{\Sigma}$. Additionally, from Equation (B-4c), we have that $\boldsymbol{\Sigma}\boldsymbol{\alpha}_k = \lambda\boldsymbol{\alpha}_k$, therefore, the variance of z_k can be expressed as:

$$\mathrm{Var}[z_k] = \boldsymbol{\alpha}'_k \boldsymbol{\Sigma} \boldsymbol{\alpha}_k = \boldsymbol{\alpha}'_k \lambda \boldsymbol{\alpha}_k = \lambda \tag{B-6}$$

Here we have an important breaking point in PCA theory. We can conclude that the maximum variance of the element z_k is equal to an eigenvalue of the covariance matrix $\boldsymbol{\Sigma}$ and its corresponding eigenvector is the own $\boldsymbol{\alpha}_k$ vector of weights. As $\boldsymbol{\Sigma}$ has p eigenvalues, to guarantee that $\mathrm{Var}[z_1] \geq \mathrm{Var}[z_2] \geq \cdots \geq \mathrm{Var}[z_p]$, $\mathrm{Var}[z_k]$ is equal to the greatest kth eigenvalue of $\boldsymbol{\Sigma}$. Thus, we can define all p PCs in vector $\boldsymbol{z}$, sorted in descending order of variance by finding $\boldsymbol{\Sigma}$ eigenvalues and their corresponding eigenvectors. With that, most of the variance information regarding the original variables is contained in the firsts PCs of vector $\boldsymbol{z}$.

At last, we can define the vector of PCs by the following matrix notation:

$$\boldsymbol{A} = \begin{bmatrix} | & | & & | \\ \boldsymbol{\alpha}_1 & \boldsymbol{\alpha}_2 & \dots & \boldsymbol{\alpha}_p \\ | & | & & | \end{bmatrix} \tag{B-7}$$

$$\boldsymbol{z} = (z_1, z_2, \dots, z_p)' \tag{B-8}$$

$$\boldsymbol{z} = \boldsymbol{A}'\boldsymbol{x} \tag{B-9}$$

where $\boldsymbol{A}$ is a matrix where each kth column is composed by the kth weight vector $\boldsymbol{\alpha}_k$.

B.2
Sample Principal Components

In practical applications, we don't know the whole population of the random variables involved. However, what we do have are samples of these populations. Therefore, principal components are derived by considering the sample variation metrics. In this section, we demonstrate how principal com-

ponents were extracted is these dissertation studies.

In this work, we want to extract the PCs of samples of the system loads. Therefore, we have as input a $\tilde{\boldsymbol{X}}_{M \times N}$ matrix where each row m is related to a system load and each column n is related to a sample. In this manner, it is our interest to obtain a $\boldsymbol{Z}_{T \times N}$ matrix where $T \leq M$ and each row of this matrix refers to a principal component of the load matrix $\tilde{\boldsymbol{X}}$.

To extract $\boldsymbol{Z}$ we do as follows:

– First, we center the input data $\tilde{\boldsymbol{X}}$ by subtracting each row element by the mean value of that row.

$$X_{mn} = \tilde{X}_{mn} - \overline{X}_m \qquad \forall\, m = 1, \ldots, M;\, n = 1, \ldots, N \qquad \text{(B-10)}$$

where,

$$\overline{X}_m = \frac{1}{N} \sum_{n=1}^{N} \tilde{X}_{mn} \qquad \forall\, m = 1, \ldots, M \qquad \text{(B-11)}$$

– Them we calculate the covariance matrix $\boldsymbol{S}_{M \times M}$ for the centered samples in $\boldsymbol{X}$.

$$S_{ij} = \frac{1}{N-1} \sum_{n=1}^{N} X_{in} X_{jn} \qquad \forall\, i = 1, \ldots, M;\, j = 1, \ldots, M \qquad \text{(B-12)}$$

– For the covariance matrix $\boldsymbol{S}$ we calculate its eigenvalues $\{\lambda_m\}_{m=1}^{M}$ and corresponding eigenvectors $\{\boldsymbol{a}_m\}_{m=1}^{M}$ by solving the equation below.

$$(\boldsymbol{S} - \lambda_m \boldsymbol{I})\boldsymbol{a}_m = 0 \qquad \text{(B-13)}$$

– At this point, we can order the eigenvector in the columns of an $\boldsymbol{A}_{N \times M}$ matrix. The eigenvector related to the greatest eigenvector is in the first column of $\boldsymbol{A}$. Thus, the other eigenvectors are sorted in a descending order of λ. As a result, the lasts columns contain the eigenvectors with the smallest eigenvalues associated.

$$\boldsymbol{A} = \begin{bmatrix} | & | & & | \\ \boldsymbol{a}_1 & \boldsymbol{a}_2 & \ldots & \boldsymbol{a}_M \\ | & | & & | \end{bmatrix} \qquad \text{(B-14)}$$

Finally, with $\boldsymbol{A}$ and $\boldsymbol{X}$ we calculate the $\boldsymbol{Z}$ matrix of principal components.

$$\boldsymbol{Z} = \boldsymbol{A}'\boldsymbol{X} \qquad \text{(B-15)}$$

– However, in our applications we want PCA to reduce the dimension of our data matrices. Therefore, we abdicate of fully representing the variance of the input data to represent only a percentage of this variance. In this manner, we select the first T components that represent at least α percent of the total variance.

$$\alpha \leq \frac{\sum_{i=1}^{T} \lambda_i}{\sum_{j=1}^{M} \lambda_j} \times 100\% \qquad \text{(B-16)}$$

C
References

[1] A. Velloso, D. Pozo, and A. Street, "Distributionally robust transmission expansion planning: a multi-scale uncertainty approach," *eprint arXiv:1810.05212*, pp. 1–12, 2018.

[2] A. Velloso, A. Street, D. Pozo, J. M. Arroyo, and N. G. Cobos, "Two-stage robust unit commitment for co-optimized electricity markets: An adaptive data-driven approach for scenario-based uncertainty sets," *IEEE Transactions on Sustainable Energy*, pp. 1–1, 2019.

[3] N. G. Cobos, J. M. Arroyo, N. Alguacil, and A. Street, "Network–constrained unit commitment under significant wind penetration: A multistage robust approach with non-fixed recourse," *Applied Energy*, vol. 232, pp. 489–503, 2018. [Online]. Available: http://www.sciencedirect.com/science/article/pii/S0306261918314132

[4] N. G. Cobos, J. M. Arroyo, N. Alguacil, and A. Street, "Robust energy and reserve scheduling under wind uncertainty considering fast-acting generators," *IEEE Transactions on Sustainable Energy*, vol. 10, no. 4, pp. 2142–2151, Oct 2019.

[5] A. M. Leite da Silva and A. M. de Castro, "Risk assessment in probabilistic load flow via monte carlo simulation and cross-entropy method," *IEEE Transactions on Power Systems*, vol. 34, no. 2, pp. 1193–1202, March 2019.

[6] J. J. Grainger, W. D. Stevenson, W. D. Stevenson *et al.*, *Power system analysis*, 2003.

[7] B. Stott, J. Jardim, and O. Alsac, "Dc power flow revisited," *IEEE Transactions on Power Systems*, vol. 24, no. 3, pp. 1290–1300, Aug 2009.

[8] Y. Qi, D. Shi, and D. Tylavsky, "Impact of assumptions on dc power flow model accuracy," in *2012 North American Power Symposium (NAPS)*, Sep. 2012, pp. 1–6.

[9] S. H. Low, "Convex relaxation of optimal power flow—part i: Formulations and equivalence," *IEEE Transactions on Control of Network Systems*, vol. 1, no. 1, pp. 15–27, March 2014.

[10] ——, "Convex relaxation of optimal power flow—part ii: Exactness," *IEEE Transactions on Control of Network Systems*, vol. 1, no. 2, pp. 177–189, June 2014.

[11] J. B. Ward, "Equivalent circuits for power-flow studies," *Transactions of the American Institute of Electrical Engineers*, vol. 68, no. 1, pp. 373–382, July 1949.

[12] A. Monticelli, S. Deckmann, A. Garcia, and B. Stott, "Real-time external equivalents for static security analysis," *IEEE Transactions on Power Apparatus and Systems*, vol. PAS-98, no. 2, pp. 498–508, March 1979.

[13] S. Deckmann, A. Pizzolante, A. Monticelli, B. Stott, and O. Alsac, "Numerical testing of power system load flow equivalents," *IEEE Transactions on Power Apparatus and Systems*, vol. PAS-99, no. 6, pp. 2292–2300, Nov 1980.

[14] F. Wu and A. Monticelli, "Critical review of external network modelling for online security analysis," *International Journal of Electrical Power & Energy Systems*, vol. 5, no. 4, pp. 222–235, 1983, special Issue Control Centres. [Online]. Available: http://www.sciencedirect.com/science/article/pii/0142061583900236

[15] G. Irisarri, A. M. Sasson, and J. F. Dopazo, "Real-time external system equivalent for on-line contingency analysis," *IEEE Transactions on Power Apparatus and Systems*, vol. PAS-98, no. 6, pp. 2153–2171, Nov 1979.

[16] M. A. H. Ibrahim, O. M. Mostafa, and A. H. El-Abiad, "Dynamic equivalents using operating data and stochastic modeling," *IEEE Transactions on Power Apparatus and Systems*, vol. 95, no. 5, pp. 1713–1722, Sep. 1976.

[17] R. Podmore, "A comprehensive program for computing coherency-based dynamic equivalents," in *IEEE Conference Proceedings Power Industry Computer Applications Conference, 1979. PICA-79.*, May 1979, pp. 298–306.

[18] Y. Zhu and D. J. Tylavsky, "An optimization based generator placement strategy in network reduction," in *2014 North American Power Symposium (NAPS)*, Sep. 2014, pp. 1–6.

[19] Y. Zhu and D. Tylavsky, "An optimization based network reduction method with generator placement," in *2015 North American Power Symposium (NAPS)*, Oct 2015, pp. 1–6.

[20] N. Marinho, Y. Phulpin, D. Folliot, and M. Hennebel, "Network reduction based on multiple scenarios," in *2017 IEEE Manchester PowerTech*, June 2017, pp. 1–6.

[21] Y. Zhu and D. Tylavsky, "An optimization-based dc-network reduction method," *IEEE Transactions on Power Systems*, vol. 33, no. 3, pp. 2509–2517, May 2018.

[22] P. Fortenbacher, T. Demiray, and C. Schaffner, "Transmission network reduction method using nonlinear optimization," in *2018 Power Systems Computation Conference (PSCC)*, June 2018, pp. 1–7.

[23] A. Brigatto, A. Street, and D. M. Valladão, "Assessing the cost of time-inconsistent operation policies in hydrothermal power systems," *IEEE Transactions on Power Systems*, vol. 32, no. 6, pp. 4541–4550, Nov 2017.

[24] M. Maceiral, D. Penna, A. Diniz, R. Pinto, A. Melo, C. Vasconcellos, and C. Cruz, "Twenty years of application of stochastic dual dynamic programming in official and agent studies in brazil-main features and improvements on the newave model," in *2018 Power Systems Computation Conference (PSCC)*. IEEE, 2018, pp. 1–7.

[25] J. Machowski, A. Cichy, F. Gubina, and P. Omahen, "External subsystem equivalent model for steady-state and dynamic security assessment," *IEEE Transactions on Power Systems*, vol. 3, no. 4, pp. 1456–1463, Nov 1988.

[26] J. L. Jardim and A. M. L. da Silva, "A methodology for computing robust dynamic equivalents of large power systems," *Electric Power Systems Research*, vol. 143, pp. 513 – 521, 2017. [Online]. Available: http://www.sciencedirect.com/science/article/pii/S0378779616304783

[27] E. C. Housos, G. Irisarri, R. M. Porter, and A. M. Sasson, "Steady state network equivalents for power system planning applications," *IEEE Transactions on Power Apparatus and Systems*, vol. PAS-99, no. 6, pp. 2113–2120, Nov 1980.

[28] S. C. Savulescu, "Equivalents for security analysis of power systems," *IEEE Transactions on Power Apparatus and Systems*, vol. PAS-100, no. 5, pp. 2672–2682, May 1981.

[29] W. F. Tinney and J. M. Bright, "Adaptive reductions for power flow equivalents," *IEEE Transactions on Power Systems*, vol. 2, no. 2, pp. 351–359, May 1987.

[30] M. L. Oatts, S. R. Erwin, and J. L. Hart, "Application of the rei equivalent for operations planning analysis of interchange schedules," in *Conference Papers Power Industry Computer Application Conference*, May 1989, pp. 424–430.

[31] A. J. Monticelli, *Fluxo de carga em redes de energia elétrica*.   E. Blucher, 1983.

[32] L. R. Lima, A. M. L. da Silva, J. L. Jardim, A. M. Castro, and N. S. M. Silva, "A method to compute flexible static equivalents for very large power networks," in *2018 Simposio Brasileiro de Sistemas Eletricos (SBSE)*, May 2018, pp. 1–6.

[33] D. Klein, C. Spieker, S. Rüberg, V. Liebenau, and C. Rehtanz, "Aggregation of large-scale electrical energy transmission networks," 04 2016, pp. 1–6.

[34] M. Rafiq, D. Sharma, D. Wu, J. Jiang, and C. Kang, "Average electrical distance-based bus clustering method for network equivalence," 09 2017, pp. 1–6.

[35] Q. Ploussard, L. Olmos, and A. Ramos, "An efficient network reduction method for transmission expansion planning using multicut problem and kron reduction," *IEEE Transactions on Power Systems*, vol. PP, pp. 1–1, 05 2018.

[36] H. Oh, "A new network reduction methodology for power system planning studies," *Power Systems, IEEE Transactions on*, vol. 25, pp. 677 – 684, 06 2010.

[37] H. Oh, "Aggregation of buses for a network reduction," *IEEE Transactions on Power Systems*, vol. 27, no. 2, pp. 705–712, May 2012.

[38] D. Shi and D. J. Tylavsky, "An improved bus aggregation technique for generating network equivalents," in *2012 IEEE Power and Energy Society General Meeting*, July 2012, pp. 1–8.

[39] ——, "A novel bus-aggregation-based structure-preserving power system equivalent," *IEEE Transactions on Power Systems*, vol. 30, no. 4, pp. 1977–1986, July 2015.

[40] X. Cheng and T. Overbye, "Ptdf-based power system equivalents," *Power Systems, IEEE Transactions on*, vol. 20, pp. 1868 – 1876, 12 2005.

[41] S. Rao and D. Tylavsky, "Nonlinear network reduction for distribution networks using the holomorphic embedding method," in *2016 North American Power Symposium (NAPS)*, Sep. 2016, pp. 1–6.

[42] Shangyou Hao and A. Papalexopoulos, "External network modeling for optimal power flow applications," *IEEE Transactions on Power Systems*, vol. 10, no. 2, pp. 825–837, May 1995.

[43] A. Akhavein, M. Fotuhi-Firuzabad, R. Billinton, and D. Farokhzad, "Review of reduction techniques in the determination of composite system adequacy equivalents," *Electric Power Systems Research*, vol. 80, pp. 1385–1393, 12 2010.

[44] A. Shapovalov, C. Spieker, and C. Rehtanz, "Network reduction algorithm for smart grid applications," 09 2013, pp. 1–5.

[45] S. M. Ashraf, B. Rathore, and S. Chakrabarti, "Performance analysis of static network reduction methods commonly used in power systems," in *2014 Eighteenth National Power Systems Conference (NPSC)*, Dec 2014, pp. 1–6.

[46] HPPA, *Manual do Programa Organon*, High Performance Power System Applications.

[47] J. Bezanson, A. Edelman, S. Karpinski, and V. B. Shah, "Julia: A fresh approach to numerical computing," *SIAM review*, vol. 59, no. 1, pp. 65–98, 2017. [Online]. Available: https://doi.org/10.1137/141000671

[48] C. Coffrin, R. Bent, K. Sundar, Y. Ng, and M. Lubin, "Powermodels.jl: An open-source framework for exploring power flow formulations," in *2018 Power Systems Computation Conference (PSCC)*, June 2018, pp. 1–8.

[49] I. Dunning, J. Huchette, and M. Lubin, "Jump: A modeling language for mathematical optimization," *SIAM Review*, vol. 59, no. 2, pp. 295–320, 2017.

[50] "System data used for case studies," accessed on April. 20, 2020. [Online]. Available: https://1drv.ms/u/s!AlXmA_hef5K7g4t298byrZL_3c3HdA?e=SjapG3

[51] I. Jolliffe, "Principal component analysis springer verlag," 01 2002.

[52] L. I. Smith, "A tutorial on principal components analysis," Tech. Rep., 2002.

Algorithm 3: Performance Analysis

Result:

Inputs: σ_{in}

Create a Ward reduced network;

Create, the set of 100 scenarios $\mathcal{S}_{\text{training}}$ considering σ_{in};

Create, the set of 200 scenarios $\mathcal{S}_{\text{validation}}$ considering σ_{in};

Create, the set of 400 scenarios $\mathcal{S}_{\text{test}}$ considering σ_{in};

for α *in* $0 : 0.1 : 1$ **do**

    for x_λ *in* $-2 : 1 : 4$ **do**

        $\lambda = log(x_\lambda)$

        for α_θ *in* $\{0.25, 0.35, 0.6\}$ **do**

            Solve the EDC-NR model considering $\mathcal{S}_{\text{training}}$ for current α, λ, and α_θ;

            Calculate the EDCPF average error for the scenarios in $\mathcal{S}_{\text{validation}}$;

        end

    end

end

Select the parameter configuration that resulted the smaller average error;